THE JOURNAL OF BIOLOGICAL CHEMISTRY VOL. 291, NO. 46, pp. 24215–24230, November 11, 2016

Serine/Threonine Protein Phosphatase PstP of *Mycobacterium tuberculosis* Is Necessary for Accurate Cell Division and Survival of Pathogen*[S]

Received for publication, August 19, 2016 Published, JBC Papers in Press, October 7, 2016, DOI 10.1074/jbc.M116.754531

Aditya K. Sharma[‡§1,2], Divya Arora[¶1], Lalit K. Singh[‡], Aakriti Gangwal[‖], Andaleeb Sajid[‡3], Virginie Molle[**], Yogendra Singh[‡‖4], and Vinay Kumar Nandicoori[¶5]

From the [¶]National Institute of Immunology, Aruna Asaf Ali Marg, New Delhi-110067, India, [‡]CSIR-Institute of Genomics and Integrative Biology, Mall Road, Delhi-110007, India, the [‖]Department of Zoology, University of Delhi Delhi-110007, India, the [**]Laboratoire de Dynamique des Interactions Membranaires Normales et Pathologiques, Université Montpellier 2, CNRS, UMR 5235, Montpellier, France, and the [§]Academy of Scientific and Innovative Research (AcSIR), CSIR-IGIB, Delhi-110025, India

Edited by Sarkis Mazmanian

Protein phosphatases play vital roles in phosphorylation-mediated cellular signaling. Although there are 11 serine/threonine protein kinases in *Mycobacterium tuberculosis*, only one serine/threonine phosphatase, PstP, has been identified. Although PstP has been biochemically characterized and multiple *in vitro* substrates have been identified, its physiological role has not yet been elucidated. In this study, we have investigated the impact of PstP on cell growth and survival of the pathogen in the host. Overexpression of PstP led to elongated cells and partially compromised survival. We find that depletion of PstP is detrimental to cell survival, eventually leading to cell death. PstP depletion results in elongated multiseptate cells, suggesting a role for PstP in regulating cell division events. Complementation experiments performed with PstP deletion mutants revealed marginally compromised survival, suggesting that all of the domains, including the extracellular domain, are necessary for complete rescue. On the other hand, the catalytic activity of PstP is absolutely essential for the *in vitro* growth. Mice infection experiments establish a definitive role for PstP in pathogen survival within the host. Depletion of PstP from established infections causes pathogen clearance, indicating that the continued presence of PstP is necessary for pathogen survival. Taken together, our data suggest an important role for PstP in establishing and maintaining infection, possibly via the modulation of cell division events.

Signal sensing and transduction lead to a wide range of cellular responses and thus must be tightly regulated in pathogenic bacteria to allow optimal survival under variable conditions. A common mode of regulation of the cell's response to external cues is via phosphorylation and dephosphorylation of specific target proteins that lead to cellular responses like altered subcellular localization, protein turnover rates, and protein-protein interactions. Whereas phosphorylation events are mediated by kinases, dephosphorylations are mediated by the action of phosphatases. Bacteria are known to possess the conventional two-component systems involving phosphorylation of His residues in sensor kinases and Asp residues in the corresponding response regulators. These systems are critical for multiple physiological processes and cell survival (1, 2). In most of these systems, kinase-phosphatase activities are possessed by one bifunctional enzyme; for example, in the mycobacterial DevS/DosS system and WalRK system of *Bacillus anthracis*, DevS and WalK were shown to exhibit both kinase and phosphatase activities (3, 4). There are other known bifunctional kinase/phosphatases that do not belong to two-component systems, such as AceK of *Escherichia coli* (5) and HPr of *Bacillus subtilis* (6). Mycobacteria possess 11 two-components systems; besides this, pathogenic bacteria also possess Ser/Thr phosphorylation systems in which a protein that has been phosphorylated by a serine/threonine protein kinase (STPK)[6] would be dephosphorylated by a serine/threonine phosphatase. Analysis of the *Mycobacterium tuberculosis* whole genome sequence identified 11 eukaryotic-like STPKs (PknA–L, except for PknC), one Ser/Thr phosphatase (PstP), one tyrosine kinase (PtkA), and two tyrosine phosphatases (PtpA and PtpB) (7, 8). All of these eukaryotic-like kinases and phosphatases have now been characterized and found to be catalytically active (9–19).

Protein phosphatases belong to distinct families, and members of a family are structurally and functionally conserved enzymes. Phosphatases are classified based on the catalytic domain signature sequence they carry and their substrate preference (the metal-dependent protein phosphatase (PPM) family, the phosphoprotein phosphatase (PPP) family, and the phosphotyrosine phosphatase (PTP) family) (20, 21), and there

* This work was supported by Indo French Centre for the Promotion of Advanced Research Grant 5303-1 (to V. K. N., Y. S., and V. M.) and BSC0104 (CSIR) (to Y. S.). The authors declare that they have no conflicts of interest with the contents of this article.
[S] This article contains supplemental Table 1.
[1] Both authors contributed equally to this work.
[2] A Senior Research Fellow of the University Grants Commission, India.
[3] Present address: NIAID, National Institutes of Health, Bethesda, MD 20814.
[4] To whom correspondence may be addressed. Tel.: 91-9871095673; E-mail: ysingh@igib.res.in.
[5] To whom correspondence may be addressed. Tel.: 91-11-26703789; Fax: 91-11-26742125; E-mail: vinaykn@nii.ac.in.

[6] The abbreviations used are: STPK, serine/threonine protein kinase; Dox, doxycycline hydrochloride; PPM, metal-dependent protein phosphatase; PPP, phosphoprotein phosphatase; PTP, phosphotyrosine phosphatase; LMW, low molecular weight; ATc, anhydrotetracycline; IVN, isovaleronitrile; AES, allelic exchange substrate; SEM, scanning electron microscopy; WCL, whole cell lysate; ANOVA, analysis of variance.

are examples known from all of these families in bacteria (20, 22, 23). PPP phosphatases are predominantly found in eukaryotes and target Ser/Thr residues in their substrates. The PP2C class of Ser/Thr phosphatases belong to PPM family and require Mg^{2+}/Mn^{2+} for their activity. In most bacteria, these are usually secreted out of the cell; PTPs are the Tyr phosphatases and are subclassified into class I standard classical PTPs and class II low molecular weight (LMW-PTP), which in many bacteria are secreted into the extracellular milieu (20, 22, 23). *M. tuberculosis* encodes two tyrosine phosphatases, PtpA and PtpB. Deletion of *ptpA*, an LMW-PTP, did not impact *M. tuberculosis* growth either *in vitro* or in the mouse infection model (24). However, results from competitive co-infection of THP-1 macrophages with *H37Rv* and *Mtb*Δ*ptpA* strains revealed that PtpA is important for long term infection (25). PtpA is secreted from the bacterial cell and dephosphorylates the host's VPS33B (vacuolar protein sorting 33B) protein, a subunit of the VPS-C complex, thus causing the inhibition of phago-lysosomal fusion (25). The interaction of PtpA with the host vacuolar H^+ ATPase is necessary for the dephosphorylation of VPS33B and subsequent phagosomal exclusion of V-ATPase (26). PtpB is also secreted into the extracellular milieu, and the disruption of *ptpB* impairs the pathogen's ability to survive in activated macrophages and guinea pigs (27). Clearance of *M. tuberculosis* from the lungs occurs via endocytic pathways that require the fusion of phagosome with lysosome, mediated by the VPS-C complex (28). Although no direct substrates of PtpB have been identified to date, the expression of PtpB in activated macrophages attenuated IFN-γ and IL-6 production, possibly through ERK2 and p38 dephosphorylation (29).

The lone serine/threonine phosphatase of *M. tuberculosis*, PstP, belongs to the PP2C class of PPM family phosphatases and strictly requires the Mn^{2+} ion for its activity (30). The enzyme localizes to the cell membrane and contains a 240-amino acid intracellular catalytic domain, tethered via a single transmembrane helix to the 196-amino acid-long extracellular domain (18, 31). Although two metal centers are found in the catalytic core in most PP2C phosphatases, the crystal structural of PstP showed the presence of three metal-binding centers (31). The structure of PstP was later refined by the analysis of the trigonal crystal form, which has a similar core structure as the monoclinic crystal but a different flap region (32). The active site residues are conserved between the eukaryotic phosphatase PP2Cα and the PstP (31). The conserved active site residues Asp-38 and Asp-229 are involved in metal binding, whereas Arg-20 is involved in binding with the phosphate moiety in the target proteins, thus bridging together to stabilize the active structure of the complex (31).

The PstP-encoding gene is located in an operon that encodes for essential kinases PknA and PknB, which show similar expression profiles (7, 33, 34). Previous data from our laboratory have shown that PknA and PknB phosphorylate PstP on specific residues in its cytosolic domain, and this phosphorylation is influenced by the presence of Zn^{2+} ions and inorganic phosphate (P_i). The phosphatase-dead PstP mutants ($PstP_c^{D38G}$, $PstP_c^{D229G}$, and $PstP_c^{R20G}$) are more efficiently phosphorylated by PknA and PknB. Importantly, we found that the phosphorylated PstP is more active compared with its unphosphorylated counterpart (35), suggesting a possible reverse regulation mediated through phosphorylation cascades by STPKs. Investigations carried out thus far are *in vitro* studies using purified PstP. Initial high throughput data suggested that under *in vitro* culture, *pstP* is nonessential, but the same group using Himar-based transposon mutagenesis indicated that it might be essential for growth (36, 37). The present study aims to investigate the impact of PstP overexpression or depletion on the growth of the pathogen and its survival within the host. To examine these aspects, conditional gene replacement mutants of *pstP* have been generated in both *Mycobacterium smegmatis* and *M. tuberculosis*. Using these mutants, we investigated the role of various domains of PstP in modulating cellular events, cell division, and host adaptation.

Results

Impact of Overexpression of PstP—Our laboratory has previously shown that overexpression of PknA or PknB results in cell death, probably due to hyperphosphorylation of substrates critical in modulating cell survival. Because PstP is the sole phosphatase in *M. tuberculosis*, we speculated that overexpression of PstP would also be likely to impact cell survival. To test this hypothesis, PstP was cloned into the IVN-inducible episomal vector pNit-1 (36) and tet-regulatable integrative vector pST-KirT (37). The constructs were suitably prepared and electroporated into the *M. smegmatis* mc^2155 strain, and the recombinants were analyzed for PstP expression in the presence or absence of inducer. In the case of mc^2::*KirT-pstP* strain, we noticed moderate levels of overexpression in the absence of anhydrotetracycline (ATc) (Fig. 1*A*), which was consistently observed in four independent experiments. The expression was reduced significantly upon the addition of ATc (albeit not to the endogenous levels), indicating that the promoter could be turned off upon the addition of inducer (Fig. 1*A*). Based on the growth pattern analysis, we concluded that mild overexpression of PstP from the integrative pST-*KirT-pstP* does not alter the growth profile (Fig. 1*B*). To quantitate the differences, cfu at 0 and 30 h were enumerated (Fig. 1*C*). The presence or absence of ATc did not alter the cfu obtained in the case of mc^2, suggesting that the presence of ATc is not toxic to the cells. Analysis suggested that the mild overexpression of PstP in mc^2::*KirT-pstP* strain did not impact the number of cfu (Fig. 1*E*). Interestingly, even this level of expression led to a statistically significant increase in the cell length, which reverted back upon the addition of ATc (Fig. 2, *A* and *B*).

The results obtained for mc^2::*pNit1-pstP* varied between two phenotypes. At times, we observed significant cell death upon the addition of IVN. Western blot analysis from such an experiment exhibited significant overexpression of PstP upon the addition of IVN (data not shown). However, on the majority of occasions, we observed a marginal difference in the growth in the absence and presence of IVN (Fig. 1*E*). Correspondingly, the Western blot analysis indicated marginal differences in the expression pattern of PstP in the absence and presence of IVN (Fig. 1*D*). To quantitate the impact of PstP overexpression on cell survival, cfu analysis was performed with mc^2 and mc^2::*pNit1-pstP* cultures grown in the presence or absence IVN (Fig. 1*F*). We observed a marginal but statistically significant

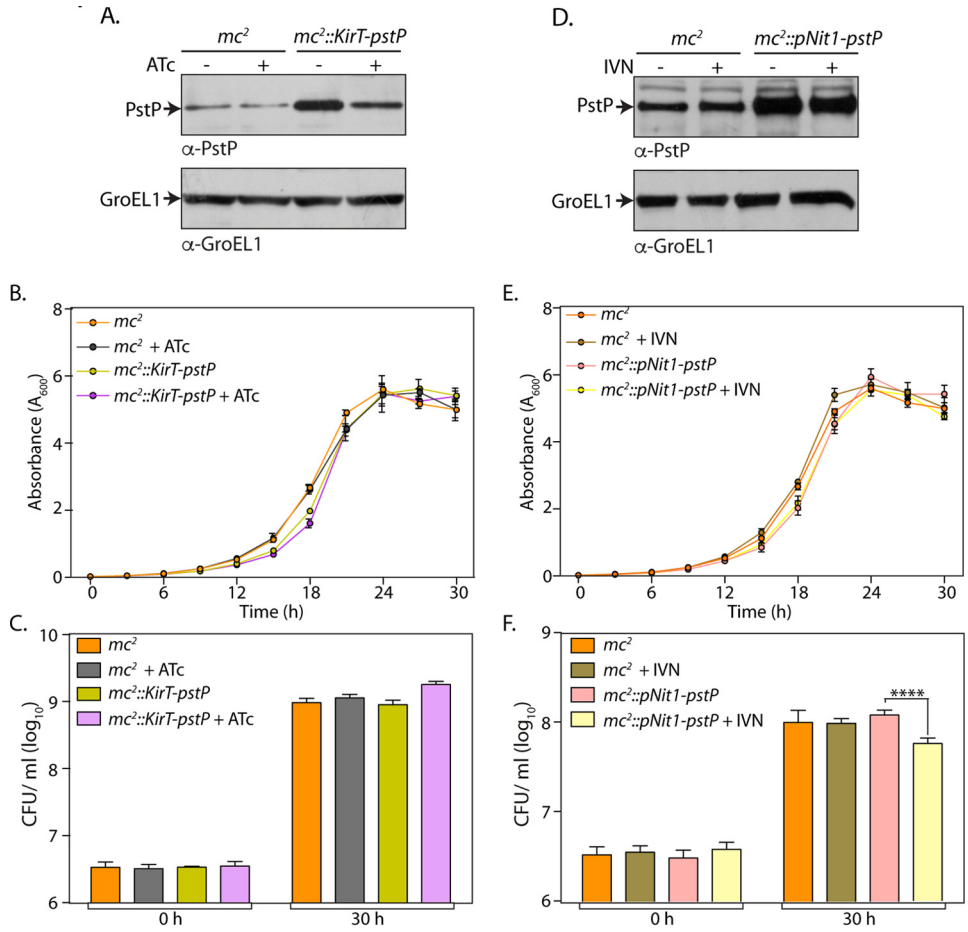

FIGURE 1. **Impact of overexpression of PstP.** *M. smegmatis* $mc^2$155 strain was electroporated with pKirT-*pstP* and pNit1-*pstP* to generate mc^2::*pKirT-pstP* and mc^2::*pNit1-pstP* strains, respectively. *A*, mc^2 or mc^2::*pKirT-pstP* cultures were initiated at an A_{600} of 0.1 and grown in the absence or the presence of 50 ng/ml ATc for 12 h. Whole cell lysates (WCLs) were prepared, and 35 μg (for PstP) and 20 μg (for GroEL1) of lysates were resolved on SDS-PAGE and probed with α-PstP and α-GroEL1 antibodies. *B*, mc^2 or mc^2::*pKirT-pstP* cultures were seeded at an initial A_{600} of 0.02 and grown in the absence or presence of 50 ng/ml ATc. Absorbance was measured every 3 h for 30 h. The experiment was performed in triplicate, the mean was plotted with the help of GraphPad Prism version 6 software, and the *error bar* represents S.D. *C*, cfu were enumerated at 0 and 30 h from the growth curve experiment in *B*. *D*, mc^2 or mc^2::*pNit1-pstP* cultures were seeded at an initial A_{600} of 0.1 and grown in the absence or presence of 5 μM IVN. WCLs were prepared and analyzed for expression of PstP and GroEL1 as described in *A*. *E* and *F*, mc^2 or mc^2::*pNit1-pstP* cultures were seeded at an initial A_{600} of 0.02 and grown in the absence or presence of 5 μM IVN. The growth curve was performed, and corresponding cfu data were analyzed and plotted as described above. ****, $p < 0.0001$, two-way ANOVA test, mean with S.D.

decrease in the cfu upon the addition of IVN (Fig. 1*F*). Scanning electron microscopy revealed that overexpression of PstP resulted in elongation of cells (Fig. 2, *C* and *D*). The presence or absence of ATc or IVN did not alter the cell length of mc^2. Interestingly, we observed slight but statistically significant change in mean cell length upon the addition of IVN (Fig. 2*D*). These results suggest a role for PstP in maintaining normal cell lengths.

Depletion of PstP in M. smegmatis Leads to Cell Death—To decipher the role of PstP in regulating cellular events, we began with creating a conditional gene replacement *pstP* mutant in *M. smegmatis*. Previous attempts to generate mycobacterial *pstP* gene replacement mutants in our laboratory were unsuccessful, possibly due to polarity effects on the expression of the downstream genes in the operon. We therefore modified the strategy for generating the allelic exchange substrate (AES), wherein the carboxyl terminus of the *hyg*^{r} gene was fused with a spacer (encoding four glycine residues and one serine residue) followed by the last 21 nucleotides of the *pstP* gene (encoding the last seven amino acids of PstP). Because the translational stop codon of PstP overlaps with the translational start codon of RodA, we reasoned that the above strategy would minimally disrupt both transcription and translation of the downstream genes. The mc^2-*KirT-pstP* strain was electroporated with pNitA-ET to generate recombineering-proficient merodiploid strain. This strain was electroporated with blunt-ended linearized AES to replace the *pstP* at the native locus with a modified *hyg*^{r} gene. Fidelity of recombination at the native *pstP* locus was confirmed by performing PCR amplification with specific primers across the replacement junctions (Fig. 3, *A* and *B*). To determine the impact of PstP depletion on cell growth, we streaked *M. smegmatis* wild type (mc^2), merodiploid (mc^2::*KirT-pstP*), and the mutant (mc^2-*cd-pstP*) on plates in the presence or absence of ATc (Fig. 3*C*). As expected, both wild type and merodiploid strains grew regardless of the presence of ATc. However, the conditional mutant grew well only in the absence of ATc, because in the presence of ATc we did not detect any growth on plates (Fig. 3*C*). Western blot analysis of the whole cell lysates, isolated at different time points post-ATc addition, confirmed the depletion of PstP (Fig. 3*D*). To examine the pos-

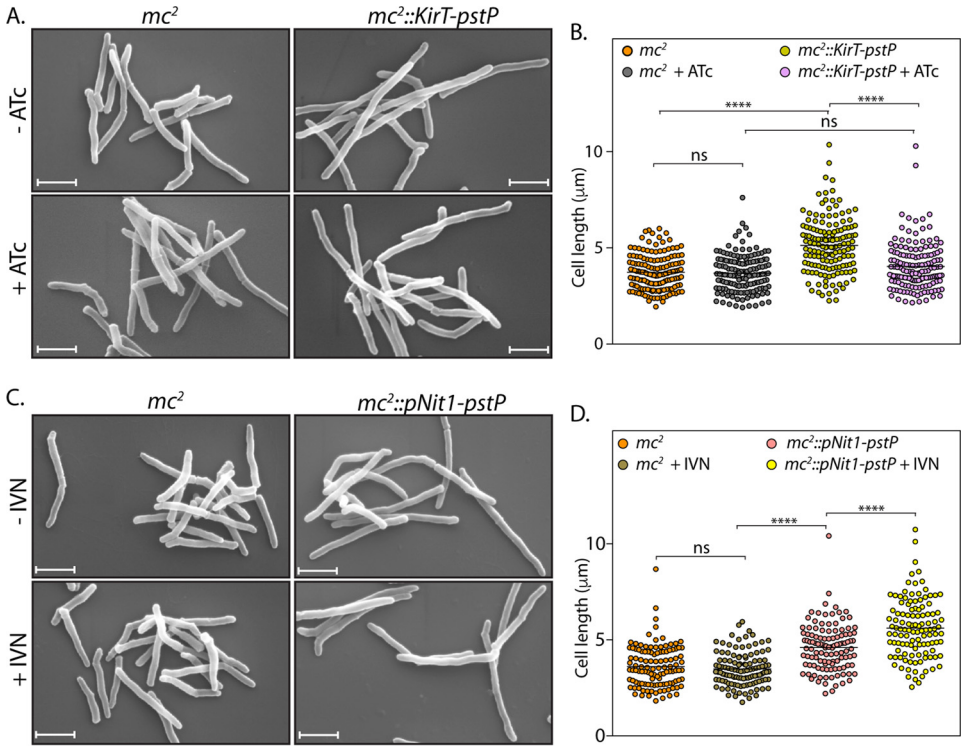

FIGURE 2. **Impact of overexpression of PstP on morphology.** *A*, mc^2 or mc^2::*KirT-pstP* cultures were seeded at 0.1 and allowed to grow in the presence and absence of 50 ng/ml ATc inducer for 12 h. Cells were processed for SEM as described under "Materials and Methods." *Scale bar*, 1 μm. *B*, cell lengths of 150 individual cells from different SEM images were measured using Smart Tiff software, and data were analyzed using GraphPad Prism version 6. Mean lengths are plotted, and significance is calculated using ordinary one-way ANOVA with $p < 0.0001$ (****). Mean lengths of mc^2, mc^2 +ATc, mc^2::*KirT-pstP* −ATc, and mc^2::*KirT-pstP* +ATc were 3.74, 3.68, 5.13, and 4.03 μm, respectively. *C*, mc^2 or mc^2::*pNit1-pstP* cultures were initiated at an A_{600} of 0.1 in the absence or presence of 5 μM IVN and grown for 12 h. SEM was performed as described. *Scale bar*, 1 μm. *D*, cell lengths of 115 individual cells from SEM images were measured by Smart Tiff software and analyzed as mentioned in *B*. Mean cell lengths of mc^2, mc^2 +IVN, mc^2::*pNit-pstP* −IVN, and mc^2::*pNit1-pstP* +IVN samples were 3.61, 3.49, 4.60, and 5.61 μm, respectively. ****, $p < 0.0001$, ordinary one-way ANOVA. *ns,* not significant.

sibility of polarity effects on the expression of downstream genes of the operon, the whole cell lysates were analyzed with anti-PknB antibody. The expression of PknB was found to be similar regardless of the presence of ATc, indicating that the replacement of *pstP* at its native locus did not alter expression of the downstream genes. A comparison of the growth pattern analysis of the mutant *versus* the wild type strain revealed that the depletion of PstP significantly reduced the growth (Fig. 3*E*). The reduced growth observed in the presence of ATc could be due to either bacteriostatic or bactericidal phenotypes. To resolve this question, we enumerated cfu at the 0 and 30 h time points in the presence and absence of ATc. The depletion of PstP resulted in ~3 log-fold decrease in the survival of bacteria, suggesting that depletion of PstP was detrimental to cell survival (Fig. 3*F*).

Decrease in PstP Expression Compromises M. tuberculosis Growth—A conditional gene replacement of *pstP* in *M. tuberculosis* was created with the help of recombineering as described under "Materials and Methods." Replacement of *pstP* at the native locus was confirmed by performing PCRs with appropriate primers (Fig. 4*A*), using the genomic DNA isolated from *Rv* and *Rv-cd-pstP* (Fig. 4*B*). Although the expression of PknB (from the last gene in the operon; Fig. 4*A*) was similar in the absence/presence of ATc, there was a significant decrease in PstP expression in the presence of ATc (Fig. 4*C*). Although this decrease in PstP expression was significant when compared with expression in the absence of ATc (compare *lanes 2* and *3* of Fig. 4*C*), the levels of PstP expression in the presence of ATc were only ~1.9-fold lower than PstP expression levels detected in wild type cells (from the native locus; compare *lane 3* with *lane 1* in Fig. 4*C*). Nevertheless, we analyzed the mutant for growth defects by determining the cfu/ml of culture grown in the absence or presence of ATc for 0, 2, and 4 days. We observed the impact of PstP decreased expression to be ~1 log-fold (10-fold) compared with the wild type (Fig. 4*D*). Thus, a tight regulation of PstP expression appears to be critical for optimal growth and survival. Moreover, scanning electron microscopy analysis indicated marginal elongation of cells upon partial depletion of PstP (Fig. 4*E*).

The Phosphatase Activity of PstP Is Essential for in Vitro Growth—PstP has four distinct domains: an intracellular catalytic domain (amino acids 1–240), a 60-amino acid-long juxtamembrane domain, a transmembrane domain that carries 18 amino acids, and an extracellular domain of 196 amino acids (Fig. 5*A*). Although the catalytic domain was shown to be functional *in vitro* (18), the roles played by the remaining domains have not been elucidated either *in vitro* or *in vivo*. To decipher the roles of the different domains and the active site residues in the functioning of PstP *in vivo*, wild type PstP, PstP deletion mutants, and PstP point mutants were cloned into pNitA. The constructs were electroporated into the *M. smegmatis* PstP conditional mutant mc^2-*cd-pstP*, and the transformants were assessed for the ability of the mutated PstP proteins (expressed from the plasmids) to complement PstP depletion (in the pres-

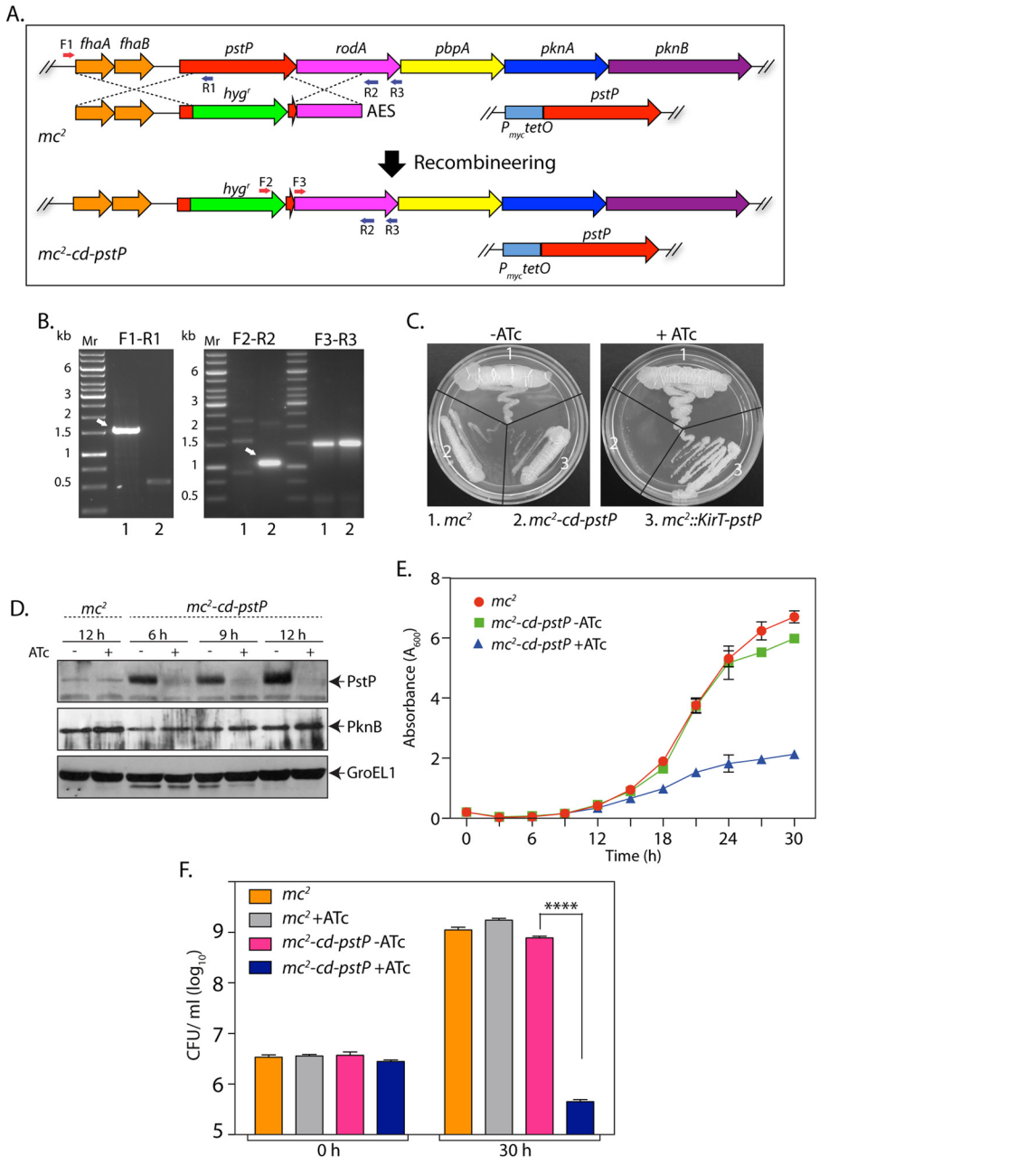

FIGURE 3. **Depletion of PstP in *M. smegmatis* leads to poor cell survival.** *A*, schematic depiction of generation of gene replacement mutant using the recombineering method. Primers used for screening the mutant are shown. *B*, agarose gels showing PCR products obtained using different primer pairs with genomic DNA obtained from mc^2 (*lane 1*) and putative mc^2-*cd-pstP* mutant (*lane 2*). F3-R3 amplifying a region of the *rodA* gene (~1.5 kb) was used as a control. *F1-R1*, ~1.5-kb fragment for mc^2 and no amplicon expected for mc^2-*cd-pstP*. *F2-R2*, no amplicon expected for mc^2 and ~1.1 kb for mc^2-*cd-pstP*. *C*, mc^2, mc^2::*pKirT-pstP*, and mc^2-*cd-pstP* cultures were grown until A_{600} reached ~0.6, and the cultures were diluted to an A_{600} of 0.1. Diluted cultures were streaked on 7H10 agar plates not containing or containing 50 ng/ml ATc. *D*, mc^2 and mc^2-*cd-pstP* cultures were initiated at an A_{600} of 0.1 and grown in the absence or presence of ATc for 6, 9, or 12 h. Whole cell lysates were isolated, resolved on SDS-PAGE, transferred to nitrocellulose membrane, and probed with α-PstP, α-PknB, and α-GroEL1 antibodies. *E*, mc^2 and mc^2-*cd-pstP* cultures were initiated at an initial A_{600} of 0.02 and grown in the absence or presence of ATc for 30 h. The experiment was performed in triplicates, and the *error bar* represents S.E. *F*, cfu were enumerated at 0 and 30 h for both mc^2 and mc^2-*cd-pstP* in the presence and absence of ATc. cfu data were analyzed and plotted as mean with S.D. (*error bars*) using GraphPad Prism version 6, and significance was calculated using two-way ANOVA with $p < 0.0001$ (****).

ence of ATc). We standardized the conditions for appropriate expression of the PstP deletion fragments by inducing with different concentrations of IVN. Western blot analysis clearly demonstrated the expression of all three deletion fragments (Fig. 5*B*, indicated by *arrows*). Growth analysis in liquid culture as well as cfu analysis suggested effective complementation by episomally expressed wild type PstP in the presence of ATc (Fig. 5, *C* and *D*). Importantly, we observed compromised growth with all three deletion mutants, and the cfu analyses are in agreement with the observed growth patterns (Fig. 5, *C* and *D*). Together, analysis suggests that although the deletion fragments could complement, the ability to complement is not equivalent to that of full-length PstP protein.

It has previously been shown that mutating Asp-38 and Asp-229 to glycine resulted in ~90% loss of the dephosphorylation activity, whereas mutating Arg-20 to Gly resulted in ~60% loss

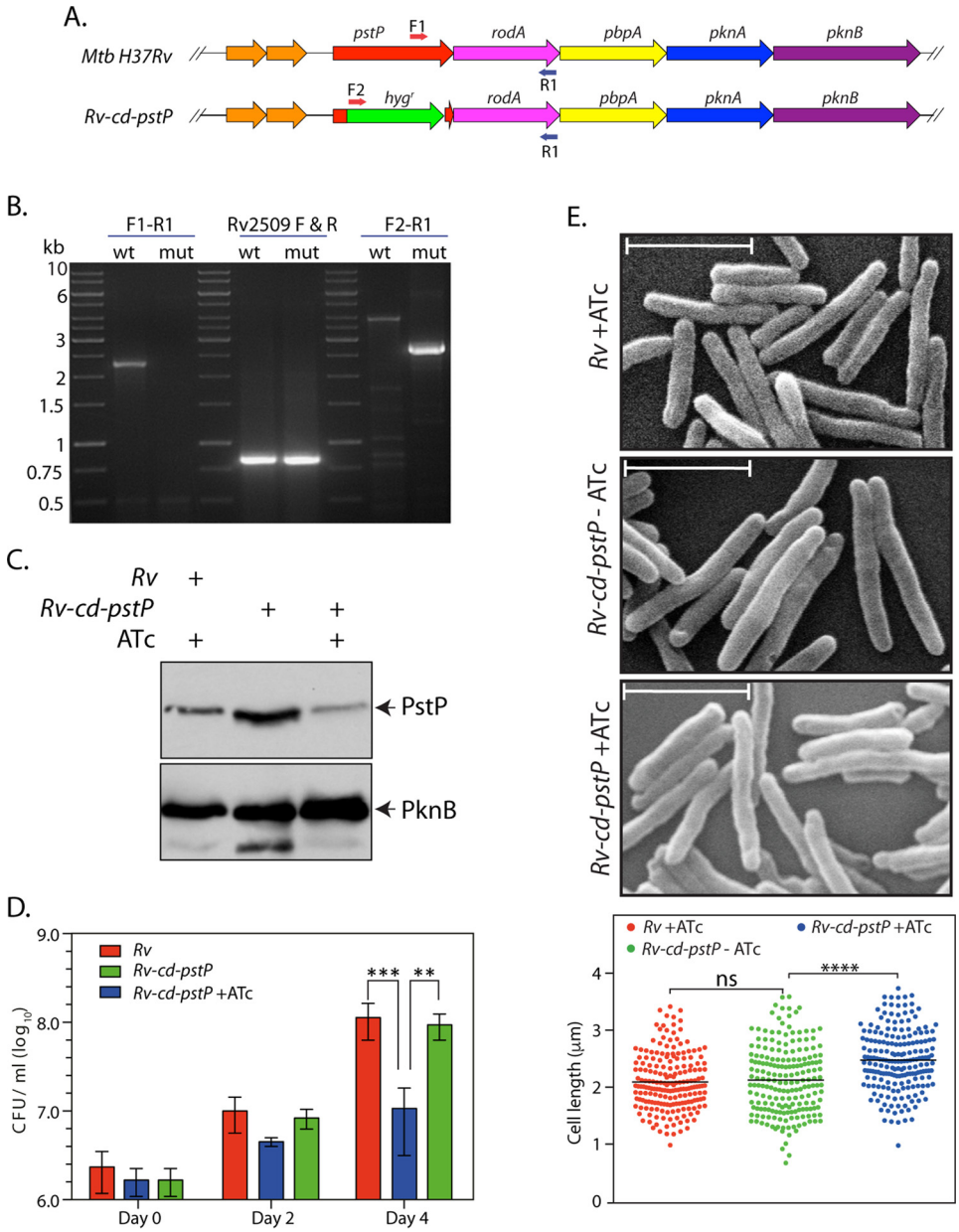

FIGURE 4. **Decrease in PstP expression compromises *M. tuberculosis* growth.** *A*, schematic representation of *Rv* and *Rv-cd-pstP* mutant. The primers used for PCR-based confirmation of the generated mutant are depicted by *arrows*. *B*, agarose gels showing the PCR amplicons obtained using genomic DNA from *Rv* (*wt*) and *Rv-cd-pstP* (*mut*). The *left panel* depicts PCR using primer F1-R1 wt (2.265 kb) and F1-R1 mut (no amplicon). The *middle panel* depicts control PCR using Rv2509 F-R primers. The *right panel* depicts PCR with F2-R1 wt (no amplicon) and F2-R1 mut (2.61 kb). *C*, *Rv* and *Rv*::*cd-pstP* cultures were initiated at an A_{600} of 0.1 and grown in the absence or presence of ATc (1 μg/ml) for 4 days. WCLs were prepared and analyzed by Western blot with α-PstP and α-PknB antibodies. *D*, *Rv* and *Rv*::*cd-pstP* cultures initiated at an A_{600} of 0.1 were grown in the presence or absence of ATc for 0, 2, or 4 days. Cultures were serially diluted and plated on 7H10 agar plates supplemented with OADC without ATc. Mean $\log_{10}$ cfu for cultures on day 4 were 8.04 cfu for *Rv*, 7.9 cfu for *Rv*::*cd-pstP* −ATc, and 6.0 cfu for *Rv*::*cd-pstP* +ATc. The experiment was performed in triplicate, and mean values with S.D. were been plotted using GraphPad Prism version 6. Significance was calculated using two-way ANOVA with $p < 0.001$ (***) and $p < 0.01$ (**). *E*, SEM analysis of *Rv*, *Rv*::*cd-pstP* −ATc, and *Rv*::*cd-pstP* +ATc cultures grown for 4 days. *Scale bar*, 1 μm. *F*, 198 cells of each cell type were visualized by SEM and measured per sample with the help of Smart Tiff software. Mean cell lengths for *Rv*, *Rv-cd-PstP* −ATc, and *Rv-cd-PstP* +ATc samples were 2.09, 2.12, and 2.47 μm, respectively. Data were plotted using GraphPad Prism version 6, and significance was calculated using two-way ANOVA with $p < 0.0001$ (****). *ns*, not significant.

of its activity (35). We sought to investigate the role of phosphatase activity of PstP in regulating growth (Fig. 6*A*). Western blot analysis of lysates prepared from the transformants confirmed the expression of PstP and its active site mutants (Fig. 6*B*). Growth pattern and cfu analysis suggested that none of the point mutants (D38G, R20G, and D229G) could complement PstP depletion (Fig. 6, *C* and *D*). Although these mutants display varying levels of residual phosphatase activity (35), it appears that a 60% loss in phosphatase activity is sufficient to compromise *in vitro* growth. Thus, our results suggest that the activity of PstP is essential for mycobacterial growth.

Depletion of PstP Results in Multiseptum Phenotype—The *pstP* gene is located in an operon that encodes for PknA, PknB, RodA, and PbpA. These four genes have all been suggested to play a critical role in cell shape maintenance, cell division, and cell wall synthesis processes (34, 38). PknA and PknB modulate

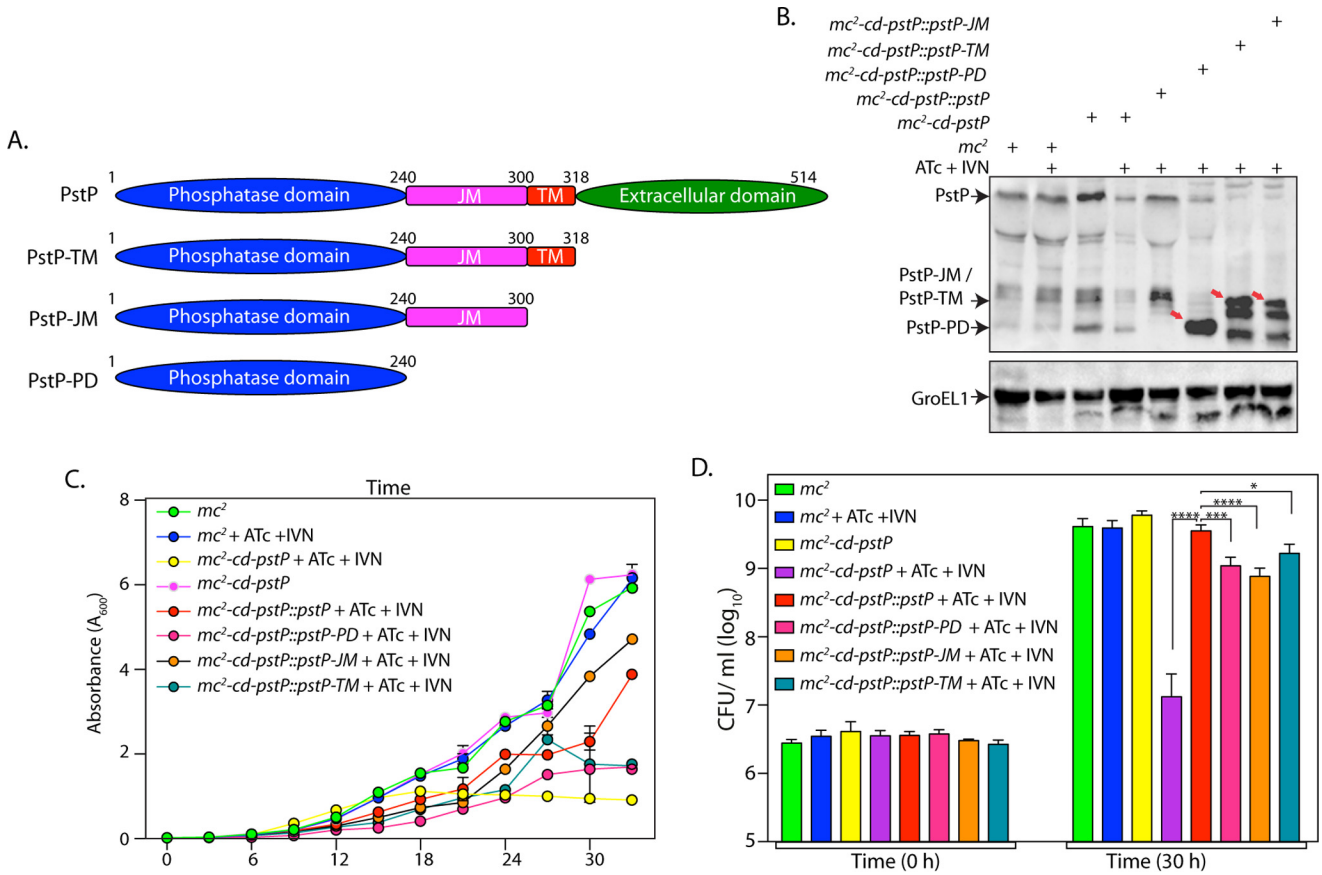

FIGURE 5. **Deletion of different PstP domains leads to mildly compromised rescue.** *A*, schematic depiction of domain structure of PstP. *PD*, phosphatase domain; *JM*, juxtamembrane; *TM*, transmembrane. *B*, *M. smegmatis* mc^2, mc^2-*cd-pstP*, mc^2-cd-*pstP*::*pstP-TM*, mc^2-cd-*pstP*::*pstP-JM*, and mc^2-*cd-pstP*::*pstP-PD* cultures were initiated at an A_{600} of 0.1 in the absence or presence of ATc + IVN (50 ng/ml ATc + 5 μM IVN) for 12 h. WCLs were prepared, and 40 μg (for PstP) and 20 μg (for GroEL1) of lysates were resolved on SDS-PAGE, transferred to nitrocellulose membrane, and probed with α-PstP and α-GroEL1 antibodies. *C*, mc^2, mc^2-*cd-pstP*, mc^2-*cd-pstP*::*pstP-TM*, mc^2-*cd-pstP*::*pstP-JM*, and mc^2-cd-*pstP*::*pstP-PD* cultures were initiated at an A_{600} of 0.02, and growth was monitored in the absence or presence of ATc + IVN every 3 h for 30 h. Growth analysis is plotted as the mean with *error bars* representing S.D. *D*, cfu enumeration was performed for mc^2, mc^2-*cd-pstP*, mc^2-cd-*pstP*::*pstP-TM*, mc^2-*cd-pstP*::*pstP-JM*, and mc^2-cd-*pstP*::*pstP-PD* from the cultures in *C* at 0 and 30 h. Data were plotted as the mean with S.D., and significance was calculated using two-way ANOVA with $p < 0.0001$ (****), $p < 0.001$ (***), and $p < 0.05$ (*).

the activities of a number of proteins that participate in cell division and cell wall synthesis by mediating their phosphorylation (39–41). Given the fact that PstP is the sole serine/threonine phosphatase in mycobacterium and is carried by an operon that carries genes controlling cell shape and cell division (including two kinases), we investigated any possible role that PstP might play in modulating cell shape and cell division by examining the impact of PstP depletion on these parameters using scanning electron microscopy (SEM). Interestingly, significantly elongated and bulged cells with multiple septa were observed in PstP-depleted samples (ATc treatment-mediated 12-h depletion), suggesting a possible role for PstP in modulating cell division (Fig. 7*A*). To confirm this phenotype, we labeled the cells with FM4–64 dye and seeded on a soft agar stage. This lipophilic dye exhibits fluorescence upon binding with the outer layer of the cell membrane, thus serving as a tool to stain and visualize plasma membranes and septa. Although the FM4-64 fluorescence pattern of mc^2-*cd-pstP* (−ATc) strain was observed to be similar to that of mc^2, we observed distinctly elongated and wider cells with multiple septa in mc^2-*cd-pstP* upon the addition of ATc (Fig. 7*B*). 198 cells of each strain were scored for their number of septa, and it was observed that there was a ~6-fold increase in multiseptate mc^2-*cd-pstP* (+ATc) cells as compared with wild type cells or mc^2-*cd-pstP* (−ATc) cells. TEM analysis revealed that the distance between two septa was much shorter than the average normal cell length in multiseptate cells (Fig. 7*D*). These results suggest the possibility that in the absence of PstP-mediated dephosphorylation of target substrates, the cells display division defects.

Depletion of PstP in M. tuberculosis Negatively Impacts Its Survival in Mice—To investigate whether stringent regulation of PstP expression is critical for the survival of pathogen within the host, we infected mice with *Rv* or *Rv-cd-pstP*, and the mice were either provided or not provided doxycycline (Fig. 8*A*). Analysis of cfu determined 1 day post-infection showed equivalent implantation of wild type and mutant bacilli in mice lungs (Fig. 8*B*). To determine the impact of PstP depletion on the survival, cfu were enumerated both in lungs and in the spleen of mice 8 weeks post-infection (Fig. 8, *B* and *C*). Gross pathological assessment of lungs at 8 weeks post-infection affirmed the presence of distinct tubercles in the lung tissue of mice infected with *Rv* and *Rv-cd-pstP* without ATc, whereas a lesser number of tubercles were observed in the case of mice infected with *Rv-cd-pstP* that were given doxycycline (Fig. 8*D*). This was also reflected in the histopathological data and scores, wherein no distinct granulomas were detected in the lungs of mice infected

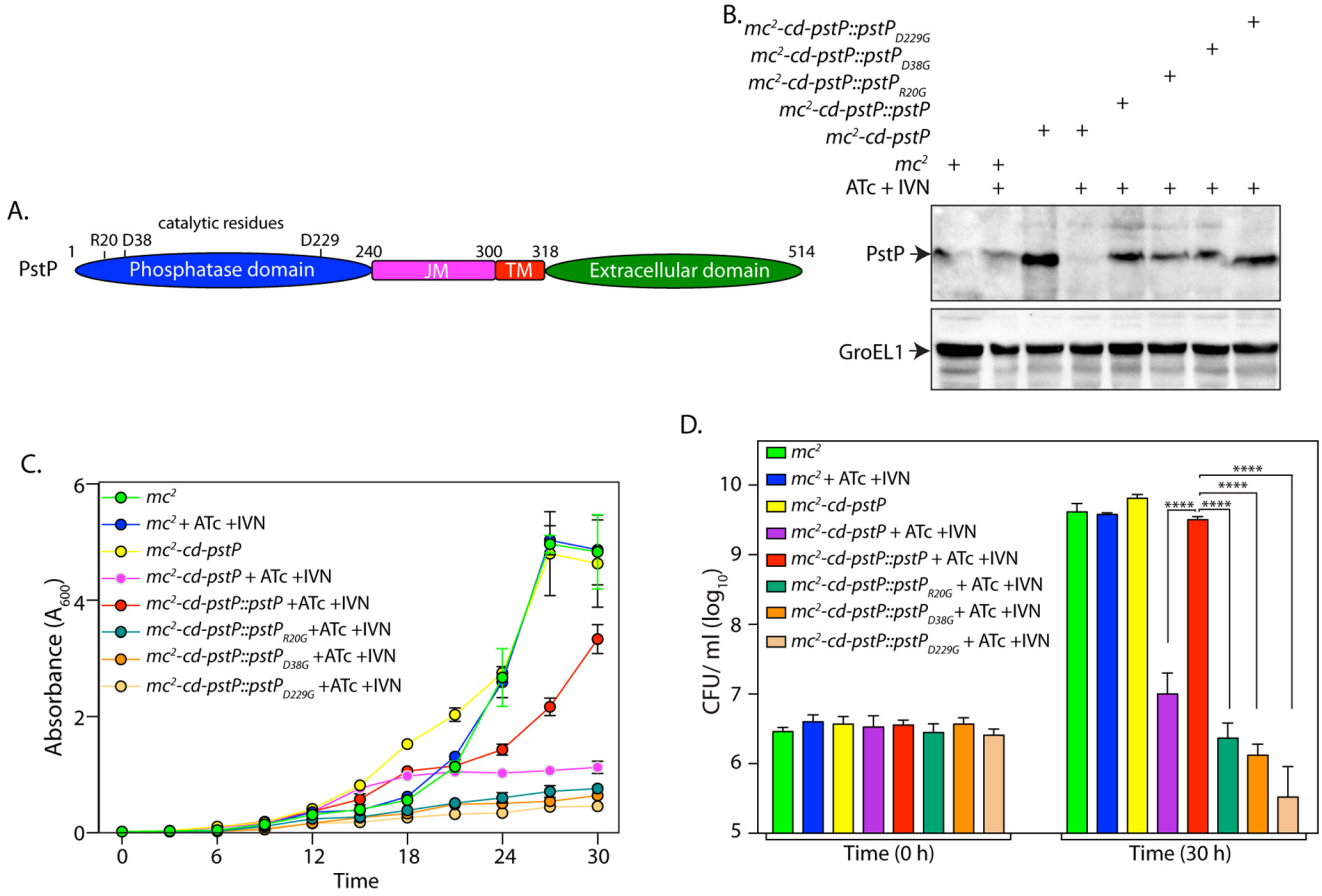

FIGURE 6. **The catalytic activity of PstP is essential for *in vitro growth*.** *A*, schematic depiction of domain structure of PstP. Residues critical for catalysis are indicated. *B*, mc^2, mc^2-*cd-pstP*, mc^2-*cd-pstP*::$pstP_{R20G}$, mc^2-*cd-pstP*::$pstP_{D38G}$, and mc^2-*cd-pstP*::$pstP_{D229G}$ strains were initiated at A_{600} of 0.1 in the absence or presence of ATc + IVN (50 ng/ml ATc + 5 μm IVN) for 12 h. WCLs were prepared, and 40 μg (for PstP) and 20 μg (for GroEL1) of lysates were resolved on SDS-PAGE and probed with α-PstP and α-GroEL1 antibodies. *C*, mc^2, mc^2-*cd-pstP*, mc^2-*cd-pstP*::$pstP_{R20G}$, mc^2-*cd-pstP*::$pstP_{D38G}$, and mc^2-*cd-pstP*::$pstP_{D229G}$ strains were seeded at an A_{600} of 0.02, and growth was monitored in the absence or presence of ATc + IVN every 3 h for 30 h. Growth analysis is plotted as the mean with *error bars* representing S.D. *D*, cfu enumeration was performed for mc^2, mc^2-*cd-pstP*, mc^2-*cd-pstP*::$pstP_{R20G}$, mc^2-*cd-pstP*::$pstP_{D38G}$, and mc^2-*cd-pstP*::$pstP_{D229G}$ strains from the cultures in *C* at 0 and 30 h. Data were plotted as the mean with S.D., and significance was calculated using two-way ANOVA with $p < 0.0001$ (****).

with *Rv-cd-pstP* +doxycycline hydrochloride (Dox) (Fig. 8, *E* and *F*). These data corroborated the cfu counts obtained in the lungs as well as the spleen 8 weeks post-infection, which were 1 log-fold (4.0 *versus* 5.1 and 4.8 for lungs and 2.1 *versus* 3.3 and 3.3 for spleen cfu) lower in mice infected with *Rv-cd-pstP* +Dox samples compared with those obtained in *Rv* and *Rv-cd-pstP* −Dox-infected mice (Fig. 8, *B* and *C*). Taken together, these results underline the importance of PstP for the survival of the pathogen in the host.

Depletion of PstP Decreases the Bacillary Load Even in an Established Infection—To determine the impact of PstP depletion on the survival of bacilli in a well established infection, we infected mice with *Rv* or *Rv-cd-pstP* and allowed the infection to progress over 4 weeks. The *Rv-cd-pstP*-infected mice were then divided into two groups, and only one group was provided Dox. Dox was also provided to *Rv* infected mice to serve as a control. The bacillary loads in the lungs and spleens of the mice were determined after 1 day, 4 weeks, and 12 weeks post-infection (Fig. 9*A*, *time line diagram*). It is apparent from the data in Fig. 9, *B* and *C*, that the bacillary load was equivalent after 1 day and 4 weeks in the case of both mice infected with *Rv* and mice infected with *Rv-cd-pstP*. Interestingly, depletion of PstP led to ~1 log-fold (3.14 *versus* 4.49 and 4.08 in lungs and 2.54 *versus* 3.57 and 3.45 in spleen cfu) decrease in the cfu both in lungs and spleen even in established infection (Fig. 9, *B* and *C*). In agreement with this observation, we noticed that the number of distinct tubercles in the lungs were lower in PstP-depleted samples (Fig. 9*D*). Histopathological analysis of lungs 12 weeks post-infection revealed the presence of a higher number of granulomas in the case of *Rv* and *Rv-cd-PstP*. However, in the presence of Dox, we observed a lower number of granulomas and correspondingly lower score in case of *Rv-cd-PstP* infection (Fig. 9, *E* and *F*). These data emphasize the need for controlled expression of PstP not only for establishment of infection (Fig. 8), but also for continued maintenance of an established infection.

Discussion

Although the eukaryotic-like phosphosignaling systems in prokaryotes are emerging as regulatory systems that are as important to the cell as their more prominent eukaryotic counterparts, the study of their functions is still in its infancy. Sensing the host environment is key to the appropriate execution of pathogen developmental programs, and mycobacterial phos-

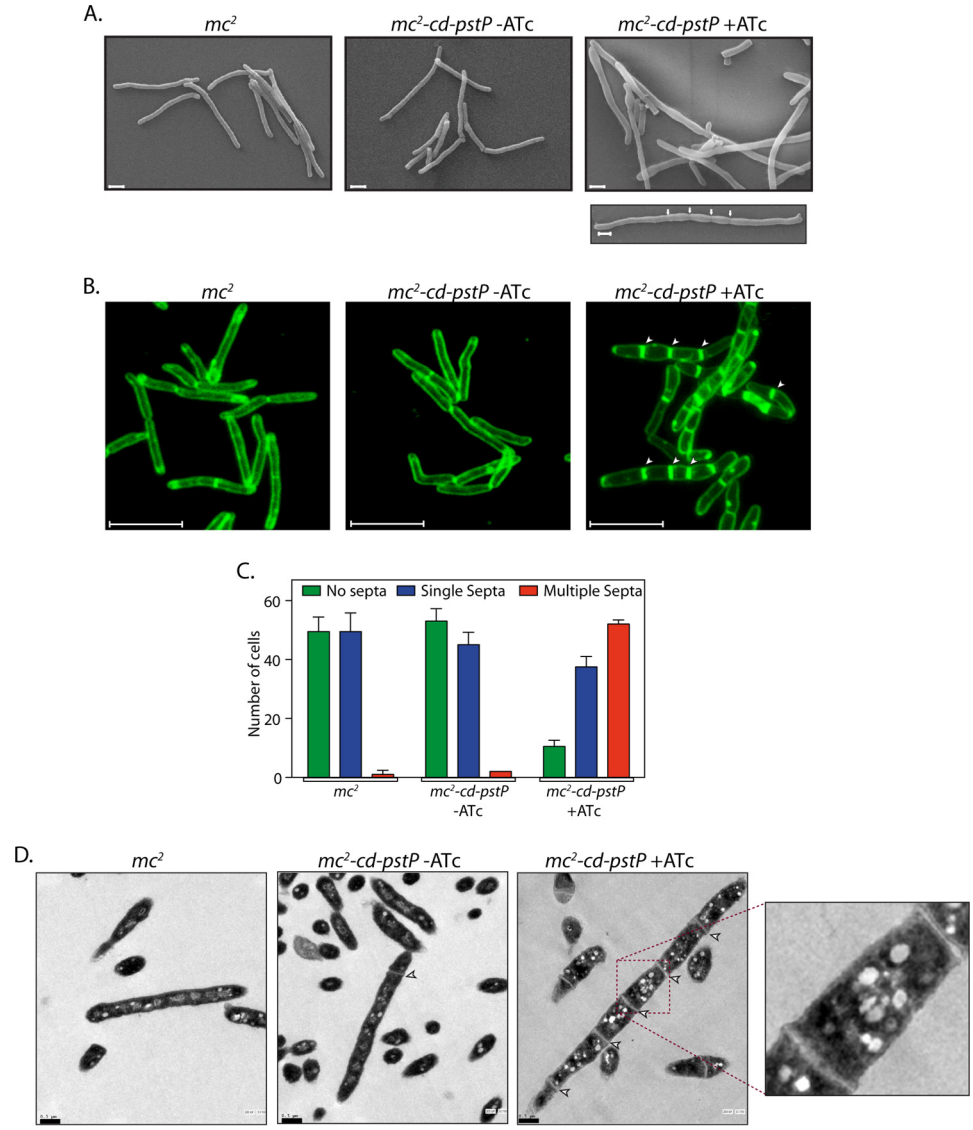

FIGURE 7. **Depletion of PstP results in multiseptum phenotype.** *A*, SEM analysis of *mc²* and *mc²*::*cd-pstP* strains grown in the absence or presence of ATc (50 ng/ml) for 12 h was performed as described (50). *White arrows* in the *bottom right panel* indicate septa. *Scale bar*, 1 μm. *B*, FM4-64 labeling and microscopy of *mc²* and *mc²*::*cd-pstP* strains grown in the absence or presence of ATc was performed as described under "Materials and Methods." The *arrows* indicate the presence of septa. *Scale bar*, 5 μm. *C*, 100 individual cells per cell type per FM4-64 labeling experiment were scored for aseptate, uniseptate, or multiseptate phenotypes. The experiment was performed twice, and the average is represented in the graph. *D*, TEM analysis of *mc²* and *mc²*::*cd-pstP* strains grown in the absence or presence of ATc for 12 h. Processed samples were visualized on grids under FEI G2 Spirit. *Scale bar*, 0.5 μm. *Error bars*, S.D.

phatases are a major family of sensor/signaling proteins. Dephosphorylation by phosphatases is critical for regulation of serine/threonine/tyrosine protein kinase-mediated cellular signaling (42, 43). In most prokaryotes, the genes encoding STPKs and corresponding protein phosphatases are carried by the same operon, seemingly following the ratio of one phosphatase per kinase (20, 43). For example, in *Streptococcus pneumoniae*, the phosphatase PhpP interacts with the kinase StkP (the genes encoding both lying in the same operon), and the presence of the kinase is essential for appropriate phosphatase localization. Additionally, cells could only survive deletion of phosphatase gene when the kinase gene *stkP* was also deleted (44). Mycobacteria and corynebacteria, however, encode multiple kinases, but they encode for only one serine/threonine phosphatase belonging to the PPM family (7, 45). The physiological purpose of such an arrangement remains undiscovered. The present study targets the investigation of the physiological impact of overexpressing and depleting PstP on growth and survival of the pathogen both *in vitro* and *in vivo*.

Among the criteria used to classify bacteria is cell shape (46). Multiple bacterial proteins are cell shape regulators. The *pstP* is the first gene of an operon that also carries *rodA*, *pbpA*, *pknA*, and *pknB* genes. RodA, named for its role in conferring bacteria with a rodlike shape, is a putative lipid II flippase (47, 48). PbpA, although not yet characterized, is predicted to be a transpeptidase required for cross-linking peptidoglycans in the periplasm space (49). Previous studies have shown that overexpression of PknA or PknB in *M. smegmatis* or *Mycobacterium bovis* BCG leads to altered cellular morphology. Whereas the overexpression of PknB results in bulged cells, overexpression of PknA results in elongated cells (34). Moreover, overexpression of PknB is detrimental to *in vitro* growth and cell survival (50).

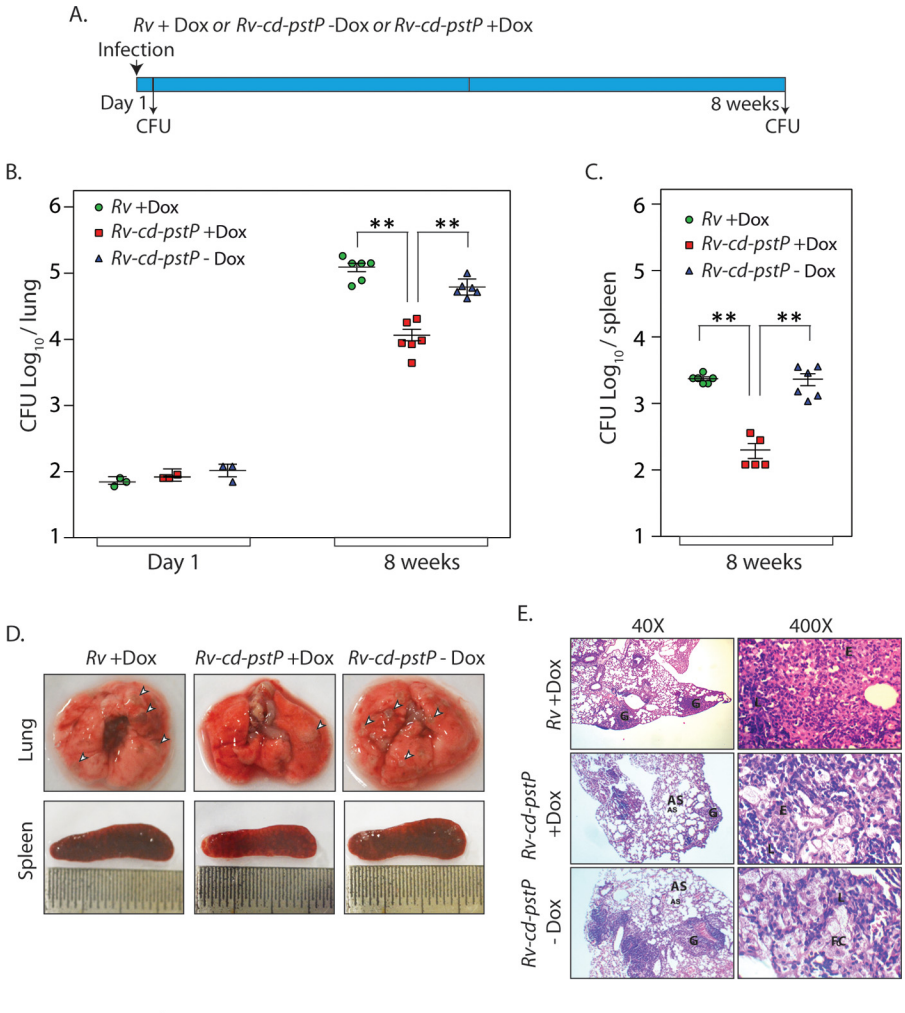

F.

Group	Bacterial Strains / treatment	No. of granulomas without necrosis Score: 2.5	Total granuloma Score
8 weeks	*Rv* + Dox	1	2.5
	Rv-cd-pstP - Dox	1	2.5
	Rv-cd-pstP + Dox	0	0

FIGURE 8. **Depletion of PstP in *M. tuberculosis* negatively impacts its survival in mice.** *A*, schematic representation of the mouse infection experiment. *B* and *C*, BALB/c mice were infected with *Rv* (9 mice) and *Rv-cd-PstP* (18 mice) as described previously (50). *Rv-cd-PstP*-infected mice were divided into two groups, and one group was provided Dox (1 mg/kg) in their drinking water. *Rv*-infected mice (9 mice) were also provided Dox in their drinking water. The water was changed every third day. Three mice from each group were sacrificed 1 day post-infection, and lung homogenates were plated in duplicates to determine mycobacterial implantation efficiency. The six remaining mice per group were sacrificed 56 days post-infection, and lung and spleen homogenates were similarly plated. *B*, the mean $\log_{10}$ cfu obtained for lung homogenates from *Rv*, *Rv-cd-PstP* +Dox, and *Rv-cd-PstP* −Dox at day 1 and day 56 were 5.1, 4.0, and 4.8 cfu, respectively. *C*, the mean $\log_{10}$ cfu obtained for spleen homogenates from *Rv* +Dox, *Rv-cd-PstP* +Dox, and *Rv-cd-PstP* at day 56 were 3.3, 2.1, and 3.3, respectively. *Error bars*, S.E. **, $p < 0.01$, two-tailed nonparametric *t* test. *D*, gross lung and spleen pathology of *Rv* +Dox-, *Rv-cd-PstP* +Dox-, and *Rv-cd-PstP*-infected mice 8 weeks post-infection. Prominent tubercles are indicated by *white arrowheads*. *E*, ×40 and ×400 images of H&E-stained lung sections of the infected mice. *G*, granuloma; *FC*, foamy cells; *AS*, alveolar space; *E*, epithelioid cells. *F*, granuloma score of the histopathology sections shown in *E*.

Our efforts to overexpress PstP using inducible nitrile promoter have not been very fruitful. Although on two occasions, we observed significant overexpression that led to cell death, in most of the experiments, we observed marginally higher expression. We do not have a good explanation for this phenomenon. We speculate that the organism found a way to make the nitrile promoter refractory to inducer concentrations. Interestingly, even with this marginal higher expression of PstP, we observed a statistically significant increase in the mean cell length (Fig. 2). Thus, it appears that the entire operon is involved in the modulation and maintenance of cell morphology and cell division.

To decipher the importance of PstP in regulating cellular events, we started with generating *M. smegmatis* and *M. tuberculosis pstP* conditional mutant strains by carrying out gene replacements (Figs. 3 and 4). The *M. smegmatis pstP* conditional mutant (*mc²-cd-pstP*) displayed almost complete depletion of PstP in the presence of ATc. This depletion of PstP was detrimental to cell survival (Fig. 3). Only partial depletion of PstP was observed in the *M. tuberculosis pstP* conditional

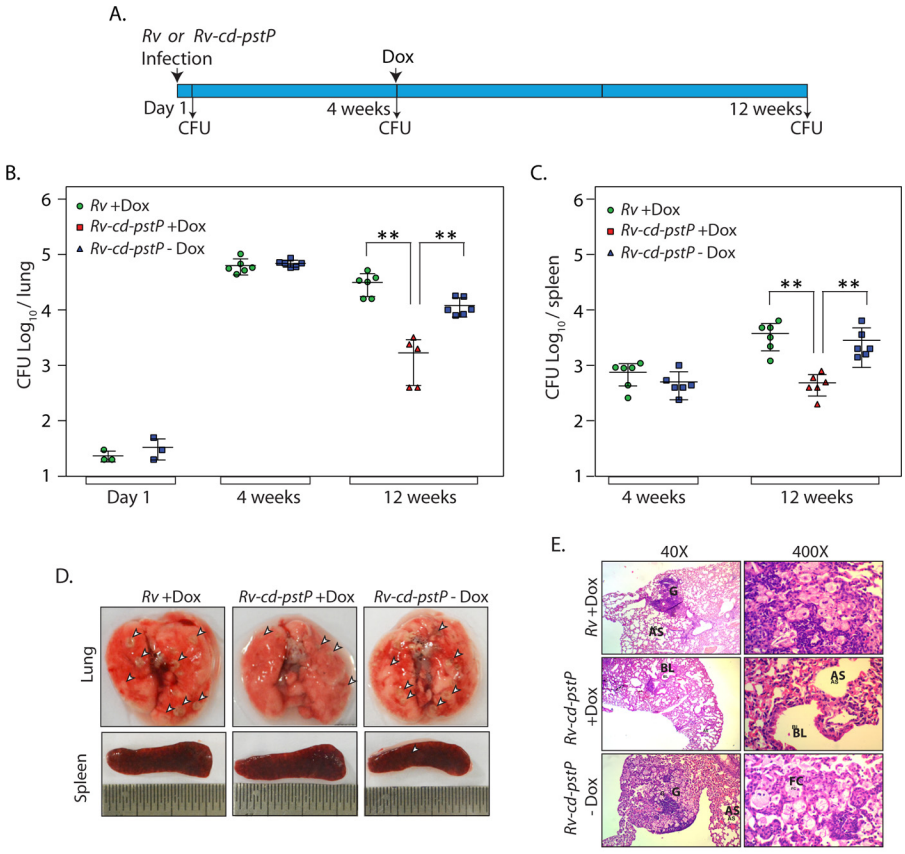

F.

Group	Bacterial Strains / treatment	No. of granulomas without necrosis Score: 2.5	Total granuloma Score
12 weeks	*Rv* +Dox	3	7.5
	Rv-cd-pstP -Dox	5	12.5
	Rv-cd-pstP + Dox	2	5

FIGURE 9. **Depletion of PstP decreases the bacillary load even in an established infection.** *A*, *schematic outline* depicting the experiment. *B* and *C*, BALB/c mice groups were infected with *Rv* and *Rv-cd-pst*. Three mice each from *Rv*- and *Rv-cd-pstP*-infected groups were sacrificed 1 day post-infection, and cfu were determined. Six mice each from *Rv* and *Rv-cd-pstP* infected groups were sacrificed 4 weeks post-infection, and the bacillary loads in the lungs and spleen were determined. Log_{10} cfu for *Rv* and *Rv-cd-pstP* in the lungs were 4.8 and 4.84, and values for the spleen were 2.66 and 2.56, respectively. *Rv-cd-pstP*-infected mice were divided into two groups ($n = 6$) 4 weeks post-infection, and one group was provided Dox (1 mg/kg) for 8 weeks. cfu were enumerated in lungs and spleen 12 weeks post-infection. The bacillary loads (log_{10} cfu) in the lungs for *Rv* + Dox, *Rv-cd-pstP* +Dox and *Rv-cd-pstP* -Dox were 4.49, 3.14, and 4.08, and bacillary loads in the spleen were 3.57, 2.54, and 3.45, respectively. *Error bars*, S.E. **, $p < 0.01$, two-tailed nonparametric *t* test. *D*, representative images of lungs and spleen after 12 weeks of infection. Prominent granulomas are indicated by *arrowheads*. *E*, ×40 and ×400 histopathology images of lung sections at 12 weeks post-infection. *G*, granuloma; *FC*, foamy cells; *AS*, alveolar space; *E*, epithelioid cells; *BL*, bronchial lumen. *F*, granuloma score of the histopathology sections of *E*.

mutant (Fig. 4), but despite this, we observed ~1 log-fold difference in cell survival, suggesting that stringent modulation of PstP expression is critical for optimal growth.

PstP and 9 of the 11 STPKs in *M. tuberculosis* contain a single transmembrane helix, connected to an extracytoplasmic domain (7, 38). The extracellular domain of PknD has been shown to be involved in sensing osmotic stress (51). The extracellular PASTA domains of PknB interact with muropeptides in the periplasmic space and are essential for *in vitro* growth of *M. tuberculosis* (50, 52). The membrane-anchoring transmembrane domain, but not the extracytoplasmic domain of PknA, is found to be essential for *in vitro* growth (53). For most mycobacterial kinases and the sole phosphatase PstP, very little is known about the functional significance of the membrane-anchoring or the extracytoplasmic domains. The phosphatase domain of PstP has been found to be necessary and sufficient for efficient catalytic activity *in vitro* (18, 35). We observed that active site mutants of PstP completely failed to rescue growth defects of the *M. smegmatis pstP* conditional mutant *in vitro*, indicating the importance of catalytically active PstP phosphatase for cell survival (Fig. 6). Similar experimental analyses with multiple other PstP mutants (Fig. 5) revealed that deletion mutants show marginally compromised survival (0.4–0.6 log-fold lower compared with the wild type). Thus, it appears that all of the domains, including the extracellular domain, are necessary for effective functional complementation.

Cell division is a complex process comprising cell elongation, septum formation, and subsequent cytokinesis, involving a myriad of proteins. Interestingly, several proteins involved in cell division and cell wall synthesis processes have been identi-

fied to be phosphorylated in phosphoproteomic studies (54–57). Among the 301 proteins identified in a high throughput phosphoproteomic study from *M. tuberculosis* H37Rv, 69 proteins were linked to cell division and cell wall synthesis processes (54). In a recent study, 398 *M. bovis* BCG proteins were identified to be phosphorylated, and 19.5% of these phosphoproteins were involved in various cellular processes (57). Similarly, phosphoproteomic analysis of *M. smegmatis mc²* and *M. bovis* BCG has revealed the phosphorylation of a number of cell division proteins, such as FtsQ, FtsW, CwsA, FtsK, and FtsY (56). Although all these proteins are important for cell division, FtsZ, a homolog of eukaryotic tubulin harboring GTPase activity, acts as a primer for divisome assembly (58). PknA phosphorylates FtsZ, thus impairing its GTPase activity and polymerization functions (59). Phosphorylation at the carboxyl terminus of FtsZ also impairs its interaction with other divisome proteins, FipA and FtsQ (59). Taken together, these studies confirm the significant role of phosphorylation in modulating the cell division process. Hence, we hypothesized that the depletion of PstP would have an impact on the cell division process. Data from scanning electron microscopy, fluorescence microscopy, and transmission electron microscopy experiments presented in Fig. 7 show the formation of multiple septa upon PstP depletion. Thus, it appears that appropriate dephosphorylation of cell division proteins is critical to orderly cell elongation and cytokinesis.

Phosphatases play an important role in determining the virulence of the pathogen. PtpA and PtpB, secretory tyrosine phosphatases of *M. tuberculosis*, have been shown to be crucial for intracellular survival of the pathogen (25, 27). However, to date, the impact of PstP depletion on mycobacterial survival in the host has not been assessed. Data from mouse infection experiments that we have carried out indicate that even partial depletion of PstP compromises pathogen survival by ~10-fold (Fig. 8). Interestingly, partial depletion of PstP from an established infection (4 weeks post-infection) also led to a ~10-fold decrease in the survival, signifying the need for continued expression of PstP for the maintenance of *M. tuberculosis* infection (Fig. 9). Specific inhibitors of PtpA and PtpB with useful IC_{50} values have been recently identified (60, 61). Standard inhibitors of PP2C phosphatases, such as cyclosporine and sodium fluoride, are not very effective against PstP. Taken together, these findings underline the importance of PstP both for *in vitro* growth and *in vivo* survival and suggest that PstP could be an effective target for therapeutic intervention.

Materials and Methods

Bacterial Strains and Reagents—A list of constructs generated and strains used in the study is presented in Table 1. Sequences and descriptions of the oligonucleotides used in the study are provided in supplemental Table 1. All medium components were purchased from BD Biosciences. Restriction endonucleases and DNA-modifying enzymes were procured from New England Biolabs and MBI Fermentas. Oligonucleotide primers and analytical grade chemicals were procured from Sigma-Aldrich or GE Healthcare. α-PstP, α-PknB, and α-GroEL-1 antibodies for immunoblotting were raised in the laboratory. Electron microscopy reagents were procured from Electron Microscopy Sciences. Doxycycline hydrochloride was purchased from Biochem Pharmaceutical (Mumbai, India). The pENTR/directional TOPO cloning kit was purchased from Invitrogen. Mycobacterial shuttle plasmids pNit-1 (Kan^r) (36), pJV53 (Kan^r) (62), and pNit-ET (Kan^r) (63) were kind gifts from Dr. Christopher Sassetti, Dr. Graham Hatfull, and Dr. Eric Rubin, respectively.

Generation of Plasmid Constructs—The *pstP* gene was amplified from *M. tuberculosis* genomic DNA with adaptor primers carrying NdeI and HindIII sites at the 5′-ends of the forward and reverse primers, respectively, using Phusion DNA polymerase (New England Biolabs). The amplicon was digested with NdeI-HindIII and cloned into the corresponding sites in pNit1 and pST-KirT (64) to generate pNit1-*pstP* and pST-KirT-*pstP* constructs, respectively. pNit1, pJV53, and pNit-ET constructs were modified by replacing the *kan^r^* gene with the *apra^r^* gene from pMV261-apra (a kind gift from Dr. William Jacobs), to generate pNitA, pJV53A, and pNitA-ET, respectively. PstP deletion mutants were created by amplifying specific fragments of the gene with adaptor primers carrying NdeI-HindIII sites and cloning the amplicons into pENTR vector. This was followed by subcloning the NdeI-HindIII fragments into the corresponding sites in pNit-apra vector. PstP point mutants created in a previous study (35) were subcloned into pNitA vector. Details of constructs used in the study are provided in Table 1.

Generation of M. smegmatis and M. tuberculosis Conditional Gene Replacement Mutants—*M. tuberculosis* H37Rv and *M. smegmatis mc²155* strains were electroporated with integration-proficient pST-KirT-*pstP* (with PstP containing an amino-terminal FLAG tag) construct, to generate merodiploid strains *Rv*::*KirT-pstP* and *mc²*::*KirT-pstP*. These strains were then electroporated with pNitA-ET and pJV53A, respectively, to generate recombineering proficient strains. These strains were electroporated. The hygromycin resistance gene (*hyg^r^*) along with its promoter was amplified from pYUB1474 construct (65) (a kind gift from Dr. William Jacobs) using adaptor primers carrying PflMI sites compatible with those found in pYUB1474. The reverse primer of *hyg^r^* was designed such that the stop codon would be replaced with an amino acid spacer (GGSGG). The amplicon obtained was cloned into pENTR vector to generate pENTR-*hyg^r^*. The apramycin resistance gene (*apra^r^*) was amplified from pMV261A and cloned into pENTR vector to generate pENTR-*apra^r^*. Upstream and downstream flanks (~1 kb on either side) of *pstP* were amplified from genomic DNA of *M. tuberculosis* and *M. smegmatis*. The forward primer of the downstream (3′) flank was designed to carry a PflMI site along with the last seven amino acids of PstP, such that these amino acids would be in frame with the *hyg^r^* gene. We also introduced an EcoRV site in the 5′-flank forward and 3′-flank reverse primers after the PflMI site. Upstream, downstream flanks digested with PflMI were ligated with the *hyg^r^* gene from pENTR-*hyg^r^*, the apramycin resistance gene from pENTR-*apra^r^*, and oriE and λcos fragment from pYUB1474 to generate allelic exchange substrates. The AES cassette containing 5′-flank-*hyg^r^*-3′-flank was released with EcoRV digestion, and the cassette was electroporated into recombineering-proficient merodiploid strains. Induction of recombineering genes before competent cell preparation was performed as described earlier (62). Con-

TABLE 1
Plasmids and strains used in the study

	Description	Source
Plasmid constructs		
pST-KirT	Integrative *Mtb* expression vector with N-terminal FLAG tag and *r-tetR* cloned in SnaBI site; Kan^r	Ref. 64
pNit-1	IVN inducible *Mtb* expression vector; Kan^r	Ref. 36
pNit-ET	Construct containing *gp60* and *gp61* genes from Che9c phase under nitrile-inducible promoter; Kan^r	Ref. 63
pJV3	Construct containing *gp60* and *gp61* genes from Che9c phase under acetamide inducible promoter; Kan^r	Ref. 62
pMV-261A	*E. coli*-mycobacterium shuttle vector, Apra^r	Kind gift from Dr. Jacobs
pNitA	pNit-1 construct wherein *kan^r* gene with the *apra^r* gene from pMV261A; Apra^r	This study
pNitA-ET	pNit-ET construct wherein *kan^r* gene was replaced with the *apra^r* gene from pMV261A; Apra^r	This study
pJV53A	pJV53 construct wherein *kan^r* gene was replaced with the *apra^r* gene from pMV261A; Apra^r	This study
pKirT-*pstP*	*pstP* cloned into NdeI-HindIII sites of pST-KirT; Kan^r	This study
pNit1-*pstP*	*pstP* cloned into NdeI-HindIII sites of pNit-1; Kan^r	This study
pNitA-*pstP*	*pstP* cloned into NdeI-HindIII sites of pNitA; Apra^r	This study
pNitA-*pstP-TM*	*pstP-TM* cloned into NdeI-HindIII sites of pNitA; Apra^r	This study
pNitA-*pstP-JM*	*pstP-JM* cloned into NdeI-HindIII sites of pNitA; Apra^r	This study
pNitA-*pstP-PD*	*pstP-PD* cloned into NdeI-HindIII sites of pNitA; Apra^r	This study
pNitA-$pstP_{R20G}$	$pstP_{R20G}$ cloned into NdeI-HindIII sites of pNitA; Apra^r	This study
pNitA-$pstP_{D38G}$	$pstP_{D38G}$ cloned into NdeI-HindIII sites of pNitA; Apra^r	This study
pNitA-$pstP_{D229G}$	$pstP_{D229G}$ cloned into NdeI-HindIII sites of pNitA; Apra^r	This study
Strains		
DH5α	*E. coli* strain used for cloning experiment	Invitrogen
mc^2	*M. smegmatis mc^{2}155* strain	ATCC, 700084
Rv	*M. tuberculosis H37Rv* strain	ATCC
Rv::pNitA-ET	*Rv* strain electroporated with pNitA-ET construct	This study
mc^2::pJV53A	*mc^2* strain electroporated with pJV53A construct	This study
mc^2::KirT-pstP	*mc^2* strain electroporated with pST-KirT-*pstP* construct	This study
Rv::KirT-pstP	*Rv* strain electroporated with pST-KirT-*pstP* construct	This study
mc^2-cd-pstP	PstP conditional mutant in *mc2::KirT-pstP* merodiploid strain	This study
Rv-cd-pstP	*PstP* conditional mutant in *Rv::KirT-pstP* merodiploid strain	This study
mc^2-cd-pstP::pstP	*mc^2-cd-pstP* strain complemented with pNitA-*pstP* construct	This study
mc^2-cd-pstP::pstP-TM	*mc^2-cd-pstP* strain complemented with pNitA-*pstP-TM* construct	This study
mc^2-cd-pstP::pstP-JM	*mc^2-cd-pstP* strain complemented with pNitA-*pstP-JM* construct	This study
mc^2-cd-pstP::pstP-PD	*mc^2-cd-pstP* strain complemented with pNitA-*pstP-PD* construct	This study
mc^2-cd-pstP::$pstP_{R20G}$	*mc^2-cd-pstP* strain complemented with pNitA-$pstP_{R20G}$ construct	This study
mc^2-cd-pstP::$pstP_{D38G}$	*mc^2-cd-pstP* strain complemented with pNitA-$pstP_{D38G}$ construct	This study
mc^2-cd-pstP::$pstP_{D229G}$	*mc^2-cd-pstP* strain complemented with pNitA-$pstP_{D229G}$ construct	This study

ditional mutants *mc^2-cd-pstP* and *Rv-cd-pstP* were screened by PCR amplification using specific primer sets to confirm that genuine recombination had occurred at the native locus (Figs. 3 and 4).

Growth Pattern Analysis—M. smegmatis mc^2 wild type and *mc^2-cd-pstP* mutant strains were electroporated with pST-KirT-pstP, pNit1-pstP, pNitA-pstP, and pNitA-$pstP_{mutant}$ (deletion mutants or point mutants) constructs to generate recombinant strains. The cultures were grown in 7H9 medium supplemented with 10% ADC (albumin, dextrose, and catalase) or in 7H10 agar medium supplemented with 10% OADC (oleic acid, albumin, dextrose, and catalase). To analyze growth on plates, cultures were diluted to an A_{600} of ~0.1 and streaked on 7H10 agar plates containing either no antibiotics or ATc (50 ng/ml). To analyze growth patterns in liquid culture, cultures were initiated in triplicates at an A_{600} of ~0.02, either in the presence or absence of ATc, and absorbance at 600 nm was measured every 3 h for 30 h. The data were plotted using GraphPad Prism version 6 software. To enumerate cfu at 0 and 30 h, cultures were harvested, washed twice with PBST (PBS containing 0.05% Tween 80), resuspended, and serially diluted, and different dilutions were plated on 7H10 agar plates containing OADC. In the case of *M. tuberculosis* (Rv) or *M. tuberculosis* mutant (*Rv-cd-pstP*), cultures were seeded at an A_{600} of ~0.1, either in the presence or absence of ATc, and cultures were grown for 4 days. cfu were determined on day 0, day 2, and day 4 on 7H10 agar plates in the absence of all antibiotics.

Western Blotting Analysis—Cultures of *M. smegmatis mc^2*, *mc^2::KirT-pstP*, *mc^2::pNit1-pstP*, *mc^2-cd-pstP*, or *mc^2-cd-pstP::*$pstP_{wt/mutant}$ strains seeded at an A_{600} of ~0.1 were grown for different times in the absence or presence of ATc or IVN or ATc + IVN. In the case of *M. tuberculosis* strains *Rv* or *Rv-cd-pstP*, cultures seeded at an A_{600} of 0.1 were grown in the absence or presence of ATc for 4 days. Whole cell lysates were isolated from harvested cells and analyzed by Western blotting as described earlier (53).

Scanning Electron Microscopy—Cultures of *M. smegmatis mc^2* or *mc^2-cd-pstP* strains were initiated at an A_{600} of 0.1 and grown for 12 h in the absence or presence of ATc in filtered 7H9 medium. Similarly, Rv and Rv-*cd-PstP* cultures were initiated at an A_{600} of ~0.1 and grown for 4 days in the absence or presence of ATc in filtered 7H9 medium. Cells were harvested, and SEM analysis was performed as described earlier (50).

Transmission Electron Microscopy—M. smegmatis mc^2 and *mc^2-cd-pstP* strains were grown until mid-log phase in the absence or presence of ATc. The cells were harvested at 4,300 × *g* and washed three times with 100 mM sodium phosphate buffer (pH 7.4). Transmission electron microscopy was performed as described earlier (66).

Immunofluorescence Analysis—FM4-64 labeling methodology was used to visualize mycobacteria by fluorescence. For this, 7H9-agarose pads were prepared on frosted slides (Corning Microslide Frosted; 75 × 25 mm) using an AB gene frame (Thermo Scientific; 17 × 54 mm). The 7H9-agarose pads comprised high resolution low melting agarose (Sigma; 1.5%) in 7H9 medium supplemented with ADC. *mc^2* or *mc^2-cd-pstP* cultures at an A_{600} of ~0.6 were diluted to an A_{600} of ~0.1, and 1 μl of diluted culture of either *mc^2* or *mc^2-cd-PstP* was spread on the

agarose pad (either with or without ATc (50 ng/ml)). The agarose pads were supplemented with FM4-64 (2 μg/ml) (67). Image acquisition was performed on a Leica TCS SP8 confocal laser scanning microscope at ×63 oil immersion with 3× optical zoom (68).

Infection of Mice with Mycobacteria—Rv and *Rv-cd-PstP* cells were grown to mid-log phase and processed, and mice were infected with these cells, as described (50). BALB/c mice of either sex that were 6–8 weeks old (obtained from the National Institute of Immunology breeding facility) were infected by the aerosol route. The lung bacillary loads were enumerated 24 h post-infection to determine the implantation dosage. For reducing PstP levels in mice infected with *Rv-cd-PstP*, Dox was supplied at a concentration of 1 mg/kg with 5% sucrose in the drinking water. Mice were dissected at the desired time point, bacillary loads were determined, and histopathology of lung sections was performed as described earlier (50).

Author Contributions—A. K. S., V. K. N., and Y. S. conceived and designed the experiments. A. K. S., D. A., A. G., and L. K. S. performed the experiments. V. K. N., Y. S., A. K. S., D. A., V. M., and A. S. analyzed the data. V. K. N., Y. S., A. S., and A. K. S. wrote the paper.

Acknowledgments—We thank the Tuberculosis Aerosol Challenge Facility (TACF) of International Center for Genetic Engineering and Biotechnology, New Delhi (ICGEB) for support in all animal experiments. We thank Dr. Dhiraj Kumar for helpful discussions and for allowing use of the TACF facility. We thank the scanning electron microscopy facility and the biocontainment facility at the National Institute of Immunology. We thank the confocal microscope facility and transmission electron microscopy facility at CSIR-Institute of Genomic and Integrative Biology. We thank Rekha Rani, Mahendra Pratap Singh, and Manish Kumar for support in SEM/TEM and confocal imaging. We thank Dr. Christopher Sassetti, Dr. Graham Hatfull, Dr. Eric Rubin, and Dr. William Jacobs for providing the plasmids.

References

1. Bourret, R. B., and Silversmith, R. E. (2010) Two-component signal transduction. *Curr. Opin. Microbiol.* **13,** 113–115
2. Stock, A. M., Robinson, V. L., and Goudreau, P. N. (2000) Two-component signal transduction. *Annu. Rev. Biochem.* **69,** 183–215
3. Kaur, K., Kumari, P., Sharma, S., Sehgal, S., and Tyagi, J. S. (2016) DevS/DosS sensor is bifunctional and its phosphatase activity precludes aerobic DevR/DosR regulon expression in *Mycobacterium tuberculosis*. *FEBS J.* **283,** 2949–2962
4. Dhiman, A., Bhatnagar, S., Kulshreshtha, P., and Bhatnagar, R. (2014) Functional characterization of WalRK: a two-component signal transduction system from *Bacillus anthracis*. *FEBS Open Bio* **4,** 65–76
5. LaPorte, D. C., and Chung, T. (1985) A single gene codes for the kinase and phosphatase which regulate isocitrate dehydrogenase. *J. Biol. Chem.* **260,** 15291–15297
6. Galinier, A., Kravanja, M., Engelmann, R., Hengstenberg, W., Kilhoffer, M. C., Deutscher, J., and Haiech, J. (1998) New protein kinase and protein phosphatase families mediate signal transduction in bacterial catabolite repression. *Proc. Natl. Acad. Sci. U.S.A.* **95,** 1823–1828
7. Cole, S. T., Brosch, R., Parkhill, J., Garnier, T., Churcher, C., Harris, D., Gordon, S. V., Eiglmeier, K., Gas, S., Barry, C. E., 3rd, Tekaia, F., Badcock, K., Basham, D., Brown, D., Chillingworth, T., Connor, R., *et al.* (1998) Deciphering the biology of *Mycobacterium tuberculosis* from the complete genome sequence. *Nature* **393,** 537–544
8. Wong, D., Chao, J. D., and Av-Gay, Y. (2013) *Mycobacterium tuberculosis*-secreted phosphatases: from pathogenesis to targets for TB drug development. *Trends Microbiol.* **21,** 100–109
9. Chaba, R., Raje, M., and Chakraborti, P. K. (2002) Evidence that a eukaryotic-type serine/threonine protein kinase from *Mycobacterium tuberculosis* regulates morphological changes associated with cell division. *Eur. J. Biochem.* **269,** 1078–1085
10. Peirs, P., Parmentier, B., De Wit, L., and Content, J. (2000) The *Mycobacterium bovis* homologous protein of the *Mycobacterium tuberculosis* serine/threonine protein kinase Mbk (PknD) is truncated. *FEMS Microbiol. Lett.* **188,** 135–139
11. Molle, V., Girard-Blanc, C., Kremer, L., Doublet, P., Cozzone, A. J., and Prost, J. F. (2003) Protein PknE, a novel transmembrane eukaryotic-like serine/threonine kinase from *Mycobacterium tuberculosis*. *Biochem. Biophys. Res. Commun.* **308,** 820–825
12. Koul, A., Choidas, A., Tyagi, A. K., Drlica, K., Singh, Y., and Ullrich, A. (2001) Serine/threonine protein kinases PknF and PknG of *Mycobacterium tuberculosis*: characterization and localization. *Microbiology* **147,** 2307–2314
13. Molle, V., Kremer, L., Girard-Blanc, C., Besra, G. S., Cozzone, A. J., and Prost, J. F. (2003) An FHA phosphoprotein recognition domain mediates protein EmbR phosphorylation by PknH, a Ser/Thr protein kinase from *Mycobacterium tuberculosis*. *Biochemistry* **42,** 15300–15309
14. Gopalaswamy, R., Narayanan, P. R., and Narayanan, S. (2004) Cloning, overexpression, and characterization of a serine/threonine protein kinase pknI from *Mycobacterium tuberculosis* H37Rv. *Protein Expr. Purif.* **36,** 82–89
15. Arora, G., Sajid, A., Gupta, M., Bhaduri, A., Kumar, P., Basu-Modak, S., and Singh, Y. (2010) Understanding the role of PknJ in *Mycobacterium tuberculosis*: biochemical characterization and identification of novel substrate pyruvate kinase A. *PLoS One* **5,** e10772
16. Kumar, P., Kumar, D., Parikh, A., Rananaware, D., Gupta, M., Singh, Y., and Nandicoori, V. K. (2009) The *Mycobacterium tuberculosis* protein kinase K modulates activation of transcription from the promoter of mycobacterial monooxygenase operon through phosphorylation of the transcriptional regulator VirS. *J. Biol. Chem.* **284,** 11090–11099
17. Lakshminarayan, H., Narayanan, S., Bach, H., Sundaram, K. G., and Av-Gay, Y. (2008) Molecular cloning and biochemical characterization of a serine threonine protein kinase, PknL, from *Mycobacterium tuberculosis*. *Protein Expr. Purif.* **58,** 309–317
18. Boitel, B., Ortiz-Lombardía, M., Durán, R., Pompeo, F., Cole, S. T., Cerveñansky, C., and Alzari, P. M. (2003) PknB kinase activity is regulated by phosphorylation in two Thr residues and dephosphorylation by PstP, the cognate phospho-Ser/Thr phosphatase, in *Mycobacterium tuberculosis*. *Mol. Microbiol.* **49,** 1493–1508
19. Koul, A., Choidas, A., Treder, M., Tyagi, A. K., Drlica, K., Singh, Y., and Ullrich, A. (2000) Cloning and characterization of secretory tyrosine phosphatases of *Mycobacterium tuberculosis*. *J. Bacteriol.* **182,** 5425–5432
20. Sajid, A., Arora, G., Singhal, A., Kalia, V. C., and Singh, Y. (2015) Protein phosphatases of pathogenic bacteria: role in physiology and virulence. *Annu. Rev. Microbiol.* **69,** 527–547
21. Shi, Y. (2009) Serine/threonine phosphatases: mechanism through structure. *Cell* **139,** 468–484
22. Shi, L., Potts, M., and Kennelly, P. J. (1998) The serine, threonine, and/or tyrosine-specific protein kinases and protein phosphatases of prokaryotic organisms: a family portrait. *FEMS Microbiol. Rev.* **22,** 229–253
23. Shi, L. (2004) Manganese-dependent protein *O*-phosphatases in prokaryotes and their biological functions. *Front. Biosci.* **9,** 1382–1397
24. Grundner, C., Cox, J. S., and Alber, T. (2008) Protein tyrosine phosphatase PtpA is not required for Mycobacterium tuberculosis growth in mice. *FEMS Microbiol. Lett.* **287,** 181–184
25. Bach, H., Papavinasasundaram, K. G., Wong, D., Hmama, Z., and Av-Gay, Y. (2008) *Mycobacterium tuberculosis* virulence is mediated by PtpA dephosphorylation of human vacuolar protein sorting 33B. *Cell Host Microbe* **3,** 316–322
26. Wong, D., Bach, H., Sun, J., Hmama, Z., and Av-Gay, Y. (2011) *Mycobacterium tuberculosis* protein tyrosine phosphatase (PtpA) excludes host

vacuolar-H^+-ATPase to inhibit phagosome acidification. *Proc. Natl. Acad. Sci. U.S.A.* **108,** 19371–19376
27. Singh, R., Rao, V., Shakila, H., Gupta, R., Khera, A., Dhar, N., Singh, A., Koul, A., Singh, Y., Naseema, M., Narayanan, P. R., Paramasivan, C. N., Ramanathan, V. D., and Tyagi, A. K. (2003) Disruption of mptpB impairs the ability of *Mycobacterium tuberculosis* to survive in guinea pigs. *Mol. Microbiol.* **50,** 751–762
28. Clarke, M., Maddera, L., Engel, U., and Gerisch, G. (2010) Retrieval of the vacuolar H-ATPase from phagosomes revealed by live cell imaging. *PLoS One* **5,** e8585
29. Zhou, B., He, Y., Zhang, X., Xu, J., Luo, Y., Wang, Y., Franzblau, S. G., Yang, Z., Chan, R. J., Liu, Y., Zheng, J., and Zhang, Z. Y. (2010) Targeting mycobacterium protein tyrosine phosphatase B for antituberculosis agents. *Proc. Natl. Acad. Sci. U.S.A.* **107,** 4573–4578
30. Chopra, P., Singh, B., Singh, R., Vohra, R., Koul, A., Meena, L. S., Koduri, H., Ghildiyal, M., Deol, P., Das, T. K., Tyagi, A. K., and Singh, Y. (2003) Phosphoprotein phosphatase of *Mycobacterium tuberculosis* dephosphorylates serine-threonine kinases PknA and PknB. *Biochem. Biophys. Res. Commun.* **311,** 112–120
31. Pullen, K. E., Ng, H. L., Sung, P. Y., Good, M. C., Smith, S. M., and Alber, T. (2004) An alternate conformation and a third metal in PstP/Ppp, the *M. tuberculosis* PP2C-family Ser/Thr protein phosphatase. *Structure* **12,** 1947–1954
32. Wehenkel, A., Bellinzoni, M., Schaeffer, F., Villarino, A., and Alzari, P. M. (2007) Structural and binding studies of the three-metal center in two mycobacterial PPM Ser/Thr protein phosphatases. *J. Mol. Biol.* **374,** 890–898
33. Narayan, A., Sachdeva, P., Sharma, K., Saini, A. K., Tyagi, A. K., and Singh, Y. (2007) Serine threonine protein kinases of mycobacterial genus: phylogeny to function. *Physiol. Genomics* **29,** 66–75
34. Kang, C. M., Abbott, D. W., Park, S. T., Dascher, C. C., Cantley, L. C., and Husson, R. N. (2005) The *Mycobacterium tuberculosis* serine/threonine kinases PknA and PknB: substrate identification and regulation of cell shape. *Genes Dev.* **19,** 1692–1704
35. Sajid, A., Arora, G., Gupta, M., Upadhyay, S., Nandicoori, V. K., and Singh, Y. (2011) Phosphorylation of *Mycobacterium tuberculosis* Ser/Thr phosphatase by PknA and PknB. *PLoS One* **6,** e17871
36. Pandey, A. K., Raman, S., Proff, R., Joshi, S., Kang, C. M., Rubin, E. J., Husson, R. N., and Sassetti, C. M. (2009) Nitrile-inducible gene expression in mycobacteria. *Tuberculosis* **89,** 12–16
37. Parikh, A., Kumar, D., Chawla, Y., Kurthkoti, K., Khan, S., Varshney, U., and Nandicoori, V. K. (2013) Development of a new generation of vectors for gene expression, gene replacement, and protein-protein interaction studies in mycobacteria. *Appl. Environ. Microbiol.* **79,** 1718–1729
38. Av-Gay, Y., and Everett, M. (2000) The eukaryotic-like Ser/Thr protein kinases of *Mycobacterium tuberculosis*. *Trends Microbiol.* **8,** 238–244
39. Molle, V., and Kremer, L. (2010) Division and cell envelope regulation by Ser/Thr phosphorylation: *Mycobacterium* shows the way. *Mol. Microbiol.* **75,** 1064–1077
40. Prisic, S., and Husson, R. N. (2014) *Mycobacterium tuberculosis* serine/threonine protein kinases. *Microbiol. Spectr.* 10.1128/microbiolspec.MGM2-0006-2013
41. Chakraborti, P. K., Matange, N., Nandicoori, V. K., Singh, Y., Tyagi, J. S., and Visweswariah, S. S. (2011) Signalling mechanisms in Mycobacteria. *Tuberculosis* **91,** 432–440
42. Böhmer, F., Szedlacsek, S., Tabernero, L., Ostman, A., and den Hertog, J. (2013) Protein tyrosine phosphatase structure-function relationships in regulation and pathogenesis. *FEBS J.* **280,** 413–431
43. Pereira, S. F., Goss, L., and Dworkin, J. (2011) Eukaryote-like serine/threonine kinases and phosphatases in bacteria. *Microbiol. Mol. Biol. Rev.* **75,** 192–212
44. Osaki, M., Arcondéguy, T., Bastide, A., Touriol, C., Prats, H., and Trombe, M. C. (2009) The StkP/PhpP signaling couple in *Streptococcus pneumoniae*: cellular organization and physiological characterization. *J. Bacteriol.* **191,** 4943–4950
45. Kalinowski, J., Bathe, B., Bartels, D., Bischoff, N., Bott, M., Burkovski, A., Dusch, N., Eggeling, L., Eikmanns, B. J., Gaigalat, L., Goesmann, A., Hartmann, M., Huthmacher, K., Krämer, R., Linke, B., *et al.* (2003) The complete *Corynebacterium glutamicum* ATCC 13032 genome sequence and its impact on the production of L-aspartate-derived amino acids and vitamins. *J. Biotechnol.* **104,** 5–25
46. Weidel, W., and Pelzer, H. (1964) Bagshaped macromolecules: a new outlook on bacterial cell walls. *Adv. Enzymol. Relat. Areas Mol. Biol.* **26,** 193–232
47. Sieger, B., Schubert, K., Donovan, C., and Bramkamp, M. (2013) The lipid II flippase RodA determines morphology and growth in *Corynebacterium glutamicum*. *Mol. Microbiol.* **90,** 966–982
48. Henriques, A. O., Glaser, P., Piggot, P. J., and Moran, C. P., Jr. (1998) Control of cell shape and elongation by the rodA gene in Bacillus subtilis. *Mol. Microbiol.* **28,** 235–247
49. Botta, G. A., and Buffa, D. (1981) Murein synthesis and β-lactam antibiotic susceptibility during rod-to-sphere transition in a pbpA(Ts) mutant of *Escherichia coli*. *Antimicrob. Agents Chemother.* **19,** 891–900
50. Chawla, Y., Upadhyay, S., Khan, S., Nagarajan, S. N., Forti, F., and Nandicoori, V. K. (2014) Protein kinase B (PknB) of *Mycobacterium tuberculosis* is essential for growth of the pathogen *in vitro* as well as for survival within the host. *J. Biol. Chem.* **289,** 13858–13875
51. Hatzios, S. K., Baer, C. E., Rustad, T. R., Siegrist, M. S., Pang, J. M., Ortega, C., Alber, T., Grundner, C., Sherman, D. R., and Bertozzi, C. R. (2013) Osmosensory signaling in *Mycobacterium tuberculosis* mediated by a eukaryotic-like Ser/Thr protein kinase. *Proc. Natl. Acad. Sci. U.S.A.* **110,** E5069–E5077
52. Mir, M., Asong, J., Li, X., Cardot, J., Boons, G. J., and Husson, R. N. (2011) The extracytoplasmic domain of the *Mycobacterium tuberculosis* Ser/Thr kinase PknB binds specific muropeptides and is required for PknB localization. *PLoS Pathog.* **7,** e1002182
53. Nagarajan, S. N., Upadhyay, S., Chawla, Y., Khan, S., Naz, S., Subramanian, J., Gandotra, S., and Nandicoori, V. K. (2015) Protein kinase A (PknA) of *Mycobacterium tuberculosis* is independently activated and is critical for growth *in vitro* and survival of the pathogen in the host. *J. Biol. Chem.* **290,** 9626–9645
54. Prisic, S., Dankwa, S., Schwartz, D., Chou, M. F., Locasale, J. W., Kang, C. M., Bemis, G., Church, G. M., Steen, H., and Husson, R. N. (2010) Extensive phosphorylation with overlapping specificity by *Mycobacterium tuberculosis* serine/threonine protein kinases. *Proc. Natl. Acad. Sci. U.S.A.* **107,** 7521–7526
55. Nakedi, K. C., Nel, A. J., Garnett, S., Blackburn, J. M., and Soares, N. C. (2015) Comparative Ser/Thr/Tyr phosphoproteomics between two mycobacterial species: the fast growing *Mycobacterium smegmatis* and the slow growing *Mycobacterium bovis* BCG. *Front. Microbiol.* **6,** 237
56. Fortuin, S., Tomazella, G. G., Nagaraj, N., Sampson, S. L., Gey van Pittius, N. C., Soares, N. C., Wiker, H. G., de Souza, G. A., and Warren, R. M. (2015) Phosphoproteomics analysis of a clinical *Mycobacterium tuberculosis* Beijing isolate: expanding the mycobacterial phosphoproteome catalog. *Front. Microbiol.* **6,** 6
57. Zheng, J., Liu, L., Liu, B., and Jin, Q. (2015) Phosphoproteomic analysis of bacillus Calmette-Guerin using gel-based and gel-free approaches. *J. Proteomics* **126,** 189–199
58. Thakur, M., and Chakraborti, P. K. (2006) GTPase activity of mycobacterial FtsZ is impaired due to its transphosphorylation by the eukaryotic-type Ser/Thr kinase, PknA. *J. Biol. Chem.* **281,** 40107–40113
59. Sureka, K., Hossain, T., Mukherjee, P., Chatterjee, P., Datta, P., Kundu, M., and Basu, J. (2010) Novel role of phosphorylation-dependent interaction between FtsZ and FipA in mycobacterial cell division. *PLoS One* **5,** e8590
60. Chiaradia, L. D., Martins, P. G., Cordeiro, M. N., Guido, R. V., Ecco, G., Andricopulo, A. D., Yunes, R. A., Vernal, J., Nunes, R. J., and Terenzi, H. (2012) Synthesis, biological evaluation, and molecular modeling of chalcone derivatives as potent inhibitors of *Mycobacterium tuberculosis* protein tyrosine phosphatases (PtpA and PtpB). *J. Med. Chem.* **55,** 390–402
61. Mascarello, A., Mori, M., Chiaradia-Delatorre, L. D., Menegatti, A. C., Delle Monache, F., Ferrari, F., Yunes, R. A., Nunes, R. J., Terenzi, H., Botta, B., and Botta, M. (2013) Discovery of *Mycobacterium tuberculosis* protein tyrosine phosphatase B (PtpB) inhibitors from natural products. *PLoS One* **8,** e77081

62. van Kessel, J. C., and Hatfull, G. F. (2007) Recombineering in *Mycobacterium tuberculosis*. *Nat. Methods* **4,** 147–152
63. Wei, J. R., Krishnamoorthy, V., Murphy, K., Kim, J. H., Schnappinger, D., Alber, T., Sassetti, C. M., Rhee, K. Y., and Rubin, E. J. (2011) Depletion of antibiotic targets has widely varying effects on growth. *Proc. Natl. Acad. Sci. U.S.A.* **108,** 4176–4181
64. Soni, V., Upadhayay, S., Suryadevara, P., Samla, G., Singh, A., Yogeeswari, P., Sriram, D., and Nandicoori, V. K. (2015) Depletion of *M. tuberculosis* GlmU from infected murine lungs effects the clearance of the pathogen. *PLoS Pathog.* **11,** e1005235
65. Jain, P., Hsu, T., Arai, M., Biermann, K., Thaler, D. S., Nguyen, A., González, P. A., Tufariello, J. M., Kriakov, J., Chen, B., Larsen, M. H., and Jacobs, W. R., Jr. (2014) Specialized transduction designed for precise high-throughput unmarked deletions in Mycobacterium tuberculosis. *MBio* **5,** e01245-14
66. Singh, L. K., Dhasmana, N., Sajid, A., Kumar, P., Bhaduri, A., Bharadwaj, M., Gandotra, S., Kalia, V. C., Das, T. K., Goel, A. K., Pomerantsev, A. P., Misra, R., Gerth, U., Leppla, S. H., and Singh, Y. (2015) clpC operon regulates cell architecture and sporulation in Bacillus anthracis. *Environ. Microbiol.* **17,** 855–865
67. Fay, A., and Glickman, M. S. (2014) An essential nonredundant role for mycobacterial DnaK in native protein folding. *PLoS Genet.* **10,** e1004516
68. de Jong, I. G., Beilharz, K., Kuipers, O. P., and Veening, J. W. (2011) Live cell imaging of *Bacillus subtilis* and *Streptococcus pneumoniae* using automated time-lapse microscopy. *J. Vis. Exp.* 10.3791/3145